Magnetic Reconnection in Plasmas

Dieter Biskamp
Max-Planck-Institut für Plasmaphysik,
85748 Garching, Germany

Abstract. A review of the present status of the theory of magnetic reconnection is given. In strongly collisional plasmas reconnection proceeds via resistive current sheets, i.e. quasi-stationary macroscopic Sweet-Parker sheets at intermediate values of the magnetic Reynolds number R_m, or mirco-current sheets in MHD turbulence, which develops at high R_m. In hot, dilute plasmas the reconnection dynamics is dominated by nondissipative effects, mainly the Hall term and electron inertia. Reconnection rates are found to depend only on the ion mass, being independent of the electron inertia and the residual dissipation coefficients. Small-scale whistler turbulence is readily excited giving rise to an anomalous electron viscosity. Hence reconnection may be much more rapid than predicted by conventional resistive theory.

Key words: Magnetic Fields, Reconnection, MHD Turbulence, Cosmic Plasmas

1. Introduction

The term magnetic reconnection derives from the simple picture of two magnetic field lines being cut and reconnected in a topologically different way. Naive as this might appear at first sight, it addresses a fundamental problem in understanding the dynamics of magnetized plasmas. Since in electrically conducting fluids the property of magnetic flux conservation gives field lines - defined as thin flux tubes - a concrete identity, which can only be destroyed by the effect of finite resistivity or some equivalent effect, magnetic reconnection processes should be slow in most astrophysical plasmas, where such non-ideal effects are extremely weak. A wide range of observations, however, indicate that large amounts of magnetic flux may be reconnected on very short time scales, which seem to be completely unrelated to the weak non-ideal processes responsible for reconnection to occur. Since rapid large-scale magnetic processes in plasmas in general require reconnection, the primary objective of reconnection theory is to identify the basic mechanisms giving rise to such fast decoupling of plasma and magnetic field. Having identified the relevant reconnection process, one may then try to understand the partition of the large-scale magnetic energy released due to fast reconnection into the different channels, i.e. heating, bulk flows and energetic particles. Since energetic particles are omni-present in astrophysical plasmas carrying a finite amount of the total plasma energy, the efficiency of particle acceleration in reconnec-

Astrophysics and Space Science **242**: 165–207, 1997.

tion processes is an important issue. A third area concerns the onset conditions for large-scale energy release by reconnection. How can free energy be stored without continuous leakage, which would only result in to some low-level dynamics, and what effect triggers the sudden large-scale release as for instance in a flare.

Most of the theoretical research on reconnection performed over the last more than thirty years deals with the first issue, i.e. to find simple configurations, usually in the framework of resistive magnetohydrodynamics (MHD), allowing efficient reconnection. After it had become clear that reconnection in a macroscopic current sheet as proposed by Sweet (1958) and Parker (1963) is far too slow to explain for instance the time scale of the flash phase of a major flare, Petschek's slow shock model (proposed at a meeting on solar flares 1964), where reconnection occurs in a micro-current sheet and thus allows reconnection rates essentially independent of the value of the resistivity, was instantly accepted as a major break-through. In fact for the following twenty years reconnection theory was focussed, at least in the western hemisphere, on Petschek's model, until its major inconsistency became apparent. The progress of the last ten years in the theory of reconnection, much as in many other branches of physics, was primarily due to numerical simulations, which allowed to study nonstationary, even turbulent configurations, to broaden the framework from resistive MHD to general two-fluid theory and even kinetic theory, and also to touch on 3-D effects, though resolution in the latter case is still only marginally adequate.

In this review, I give an overview of the present status of our perception of fast reconnection mechanisms, limiting consideration to the framework of fluid theory. In section 2, I introduce the two-fluid equations, from which the MHD approximation is easily derived. Section 3 deals with the traditional, rather well understood case of quasi stationary resistive reconnection, which takes place in macroscopic current sheets. In section 4, I then introduce several paradigmatical reconnecting systems, the tearing mode and the resistive kink mode, in particular their nonlinear behavior, the process of flux bundle coalescence, and the generation and dynamics of plasmoids. At sufficiently high magnetic Reynolds number a magnetized plasma becomes turbulent similar to the case of a neutral fluid. Small-scale turbulence makes reconnection much more efficient than in a stationary configuration. Section 5, therefore, gives an introduction to MHD turbulence. In section 6, collisionless reconnection processes are discussed, which dominate the dynamics in high temperature, dilute plasmas. In magnetized plasmas the Hall term is the dominant effect in Ohm's law, which allows a decoupling of the electrons from the ions on small scales $l < c/\omega_{pi}$. At these scales the ions

only form an immobile neutralizing background, while the dynamics is carried by the electrons, which is described by the equations of electron magnetohydrodynamics (EMHD). Reconnection rates are found to be independent of the electron dynamics, and hence depend only on the ion inertia. In the collisionless limit reconnection occurs via whistler turbulence, giving rise to anomalous electron viscosity. In section 7, I briefly discuss the other two areas, mentioned above, particle acceleration during reconnection and the problem of fast reconnection onset.

2. Two-fluid theory and the MDH approximation

The fluid description of plasmas (see, e.g. Braginskii, 1965) is a very convenient and reliable approximation of the bulk behavior, even for quasi-collisionless conditions. We are primarily interested in the long-wavelength regime $\lambda \gg \lambda_D$ (λ_D = the Debye length), where the charge density is negligible compared to the densities of ions and electrons, which is called the quasi-neutral limit. Hence the densities are equal $n_e = n_i = n$ (considering only one singly-charged ion species), which follows the continuity equation

$$\partial_t n = -\nabla \cdot \mathbf{v}_i n = -\nabla \cdot \mathbf{v}_e n \quad . \tag{1}$$

The equations of motions are

$$m_i n(\partial_t \mathbf{v}_i + \mathbf{v}_i \cdot \nabla \mathbf{v}_i) = -\nabla p_i + en(\mathbf{E} + \frac{\mathbf{v}_i}{c} \times \mathbf{B}) - \nabla \cdot \pi_i - ne\eta \mathbf{j}, \tag{2}$$

$$m_e n(\partial_t \mathbf{v}_e + \mathbf{v}_e \cdot \nabla \mathbf{v}_e) = -\nabla p_e - en(\mathbf{E} + \frac{\mathbf{v}_e}{c} \times \mathbf{B}) - \nabla \cdot \pi_e + ne\eta \mathbf{j}, \tag{3}$$

where $p_{i,e}$ are the scalar pressures, i.e. the isotropic part of the total pressure tensors, $\pi_{i,e}$ the anisotropic parts called the stress tensors. The friction term in eqs. (2), (3) is written in terms of a scalar resistivity η and the current density $\mathbf{j} = ne(\mathbf{v}_i - \mathbf{v}_e)$, which is coupled to the magnetic field by Ampeŕes law

$$\nabla \times \mathbf{B} = \frac{4\pi}{c} \mathbf{j} \, . \tag{4}$$

In the collisional-dominated case the stress tensor is given in terms of the velocity derivatives and the viscosity coefficients. For quasi-collisionless conditions no simple expression can be given for the $\pi_{i,e}$, but we assume that they are small and that the most important contribution is the residual viscosity effect, which we write in terms of simple

scalar viscosities $\mu_{i,e}$, $\nabla \cdot \pi_{i,e} = n\mu_{i,e}\nabla^2 \mathbf{v}_{i,e}$. Since heat conduction can often be neglected, the pressures follow the adiabatic law,

$$\partial_t p_{i,e} + \mathbf{v}_{i,e} \cdot \nabla p_{i,e} = -\gamma p_{i,e} \nabla \cdot \mathbf{v}_{i,e} \ . \tag{5}$$

Addition of eqs. (2) and (3) gives an equation for the mass flow $\mathbf{v} = (m_i \mathbf{v}_i + m_e \mathbf{v}_e)/(m_i + m_e) \simeq \mathbf{v}_i$, from which the electric field is eliminated:

$$m_i n(\partial_t \mathbf{v} + \mathbf{v} \cdot \nabla \mathbf{v}) = -\nabla p + \frac{1}{c}\mathbf{j} \times \mathbf{B} - \nabla \cdot \pi_i \tag{6}$$

with $p = p_i + p_e$ and $\pi_i + \pi_e \simeq \pi_i$. The electric field appears in Faraday's law

$$\partial_t \mathbf{B} = -c\nabla \times \mathbf{E} \ . \tag{7}$$

To express $\mathbf{E}$ in terms of the other dynamic quantities the electron equation of motion (3) is written in the form of a generalized Ohm's law

$$\mathbf{E} + \frac{\mathbf{v}}{c} \times \mathbf{B} = \mathbf{R}, \tag{8}$$

where $\mathbf{R}$ comprises the remaining terms. Introducing the normalizations x/L, v/v_A, t/t_A with L a typical spatial scale, $v_A = B_0/\sqrt{4\pi n m_i}$ = Alfvén velocity of a typical magnetic field B_0, $t_A = L/v_A$, $\mathbf{R}$ in eq. (8) becomes

$$\mathbf{R} = \eta \mathbf{j} + \mu_e \nabla^2 \mathbf{v}_e + d_i[\mathbf{j} \times \mathbf{B} - \beta \nabla p_e - d_e^2(\partial_t \mathbf{v}_e + \mathbf{v}_e \cdot \nabla \mathbf{v}_e)] \ , \tag{9}$$

where $d_i = c/\omega_{pi}L, d_e = c/\omega_{pe}L$ are the normalized ion and electron inertia scales, $\beta = 4\pi n T_e/B_0^2$ is a measure of the plasma pressure compared to the magnetic pressure, η is the normalized resistivity $c^2\eta/4\pi L v_A \equiv S^{-1}$, S = Lundquist number, and μ_e the normalized electron viscosity μ_e/Lv_A.

For the large-scale dynamics all terms in $\mathbf{R}$ are usually very small, e.g. $d_i \sim 10^{-7}, \eta \sim 10^{-12}$ in the solar corona, such that to lowest order $\mathbf{R} = 0$. Hence eq. (7) becomes

$$\partial_t \mathbf{B} = \nabla \times (\mathbf{v} \times \mathbf{B}) \ . \tag{10}$$

Equations (1), (5), (6), (10) are called (ideal) magnetohydrodynamics (MHD), which describe the behavior of one fluid with mass density $\rho = m_i n$, mass flow $\mathbf{v}$ and pressure p together with the magnetic field. The most important property distinguishing a highly conducting plasma from a neutral fluid is the conservation of magnetic flux across a surface

$F(t)$ bounded by a curve $l(t)$ moving with the fluid

$$\frac{d}{dt}\int \mathbf{B}\cdot d\mathbf{F} = \int_F \partial_t \mathbf{B}\cdot d\mathbf{F} + \int_{\partial_t F} \mathbf{B}\cdot d\mathbf{F} \tag{11}$$

$$= \int_F \nabla\times(\mathbf{v}\times\mathbf{B})\cdot d\mathbf{F} + \int_l \mathbf{B}\cdot(\mathbf{v}\times d\mathbf{l}) = 0 \tag{12}$$

using eq. (10) and Stokes' theorem. Sweeping the boundary curve l along $\mathbf{B}$ defines a flux tube and in the limit of vanishing tube diameter a field line. Hence in ideal MHD field lines preserve their individuality indefinitely, however strongly convoluted they may become following the fluid motion.

Observations, however, clearly indicate that most dynamic processes in plasmas involve a change of field line topology, i.e. field lines must be cut and reconnected. Since such processes, for instance solar flares or magnetospheric substorms, are very rapid, occurring on time scales close to the Alfvén time, while reconnection relies on the small flux conservation breaking effects in $\mathbf{R}$ on the right side of eq. (8), the main problem is to describe *fast* reconnection.

Conventionally, it has been assumed that reconnection requires some dissipative process. Hence the nondissipative terms in the expression (9), those proportional to d_i, have generally been ignored. Of the two dissipative effects resistivity is usually considered as the more important one, such that $\mathbf{R} \simeq \eta\mathbf{j}$. In fact most previous reconnection studies are confined to the framework of resistive MHD. In the following sections 3-5 of this review consideration is therefore restricted to this framework, while in section 6 I will discuss the conditions, when the resistive theory is no longer adequate and the collisionless effects become dominant.

In addition reconnecting motions are usually assumed to be incompressible, since they are slow compared with the phase velocities of the compressional waves, essentially v_A in a low-β plasma. This approximation simplifies the basic equations considerably. For $\nabla\cdot\mathbf{v} = 0$ the assumption of homogeneous density $n = n_0$ is consistent with the continuity equation. Taking the curl of eq. (6) eliminates the pressure. Using the same normalizations the incompressible resistive MHD equations for the vorticity $\boldsymbol{\omega}$ and $\mathbf{B}$ now become

$$\partial_t\boldsymbol{\omega} - \nabla\times(\mathbf{v}\times\mathbf{B}) - \nabla\times(\mathbf{j}\times\mathbf{B}) = \mu_i\nabla^2\boldsymbol{\omega}, \tag{13}$$

$$\partial_t\mathbf{B} - \nabla\times(\mathbf{v}\times\mathbf{B}) = \eta\nabla^2\mathbf{B}, \tag{14}$$

$$\nabla\cdot\mathbf{v} = \nabla\cdot\mathbf{B} = 0, \quad \boldsymbol{\omega} = \nabla\times\mathbf{v}, \quad \mathbf{j} = \nabla\times\mathbf{B}.$$

An important dimensionless parameter characterizing the dynamical state of a resistive fluid is the magnetic Reynolds number

$$R_m = \frac{Lv}{\eta} = S\frac{v}{v_A}, \tag{15}$$

where v is a typical average fluid velocity. Roughly speaking R_m is the ratio of the convective to the diffusive terms in eq. (14).

Since reconnection theory is often limited to 2D systems, I also give the equations for this case. With z as ignorable coordinate it is convenient to introduce the magnetic flux function ψ (essentially the vector potential component A_z) and the stream function ϕ by writing

$$\mathbf{B} = \hat{\mathbf{z}} \times \nabla\psi + \hat{\mathbf{z}}B_z, \quad \mathbf{v} = \hat{\mathbf{z}} \times \nabla\phi + \hat{\mathbf{z}}v_z,$$

such that eqs. (13), (14) become

$$\partial_t\omega + \mathbf{v}_i \cdot \nabla\omega - \mathbf{B} \cdot \nabla j = \mu_i\nabla^2\omega, \tag{16}$$

$$\partial_t\psi + \mathbf{v} \cdot \nabla\psi = \eta\nabla^2\psi, \tag{17}$$

$$\omega = \omega_z = \nabla^2\phi, \quad j = j_z = \nabla^2\psi.$$

Knowing ψ and ϕ the remaining quantities B_z, v_z, p can be computed a posteriori.

3. Quasi-stationary resistive reconnection

For $R_m \gg 1$ fast reconnection can only arise when the gradient scales occurring in the reconnection process are much shorter than the global scale L. Hence the process is localized around regions, where the convective term in eq. (14) is small, i.e. at neutral points of the magnetic configuration. For topological reasons only X-type neutral points can give rise to reconnection. Figure 1 illustrates the behavior in the vicinity of such a point, plasma flowing into the region from above and below and leaving sidewise. Figure 1 also shows that the configuration is likely to be flattened into a sheet.

In low-β systems, where only a small fraction of the total magnetic energy is available as free energy, in general only a small component of $\mathbf{B}$, the poloidal field $\mathbf{B}_\perp$, is reconnected, while the main field (assumed in z direction) remains unchanged. Hence the X-point appears only in the poloidal projection.

3.1. Basic properties of current sheets

A dynamical current sheet, usually called a Sweet-Parker sheet (Sweet, 1958; Parker, 1963), is a quasi one-dimensional stationary configuration

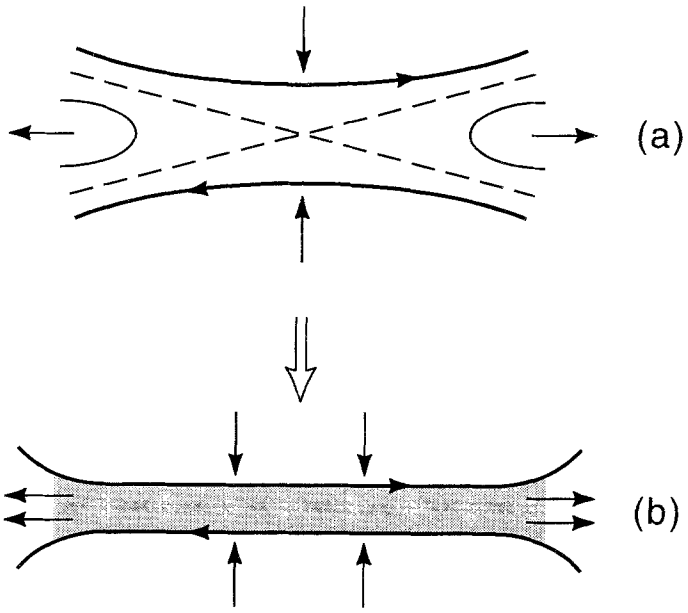

Figure 1. Reconnection flows of an X-point (a) leading to current sheet formation (b).

as illustrated in Fig.1b, where the plasma inflow balances resistive diffusion. Assuming incompressibility a current sheet is characterized by six quantities, the magnetic field immediately outside the sheet called the upstream field B_0 (the downstream field at the sheet edges is small), the upstream flow u_0 into the sheet perpendicular to the field, the downstream flow v_0 along the sheet, the width δ and the length Δ, and the resistivity η. These quantities are connected by three relations derived from the continuity equation, Ohm's law and the equation of motion, assuming stationarity. Integrating $\nabla \cdot n\mathbf{v} = n_0 \nabla \cdot \mathbf{v} = 0$ over the sheet one obtains

$$u_0 \Delta = v_0 \delta \tag{18}$$

ignoring profile effects. The z component of Ohm's law (8) with $\mathbf{R} = \eta \mathbf{j}$ and $E_z = E = \text{const.}$ gives

$$E = u_0 B_0 = \eta j \simeq \eta \frac{B_0}{\delta}. \tag{19}$$

Since in general $u_0 \ll B_0$, the inertia term is negligible in the force balance across the sheet, hence

$$B_0^2/2 = p_m - p_0, \tag{20}$$

where p_0 is the upstream pressure and p_m the pressure maximum in the sheet. Along the sheet, where the magnetic component normal to the sheet and hence the magnetic force vanish, the pressure gradient accelerates the fluid. Integration between sheet center and edge yields $v_0^2/2 = p_m - p_0$, assuming that at the edge the pressure has dropped to its upstream value. We thus obtain the important relation, that the outflow velocity equals the upstream Alfvén velocity

$$v_0 = B_0 = v_A \ . \tag{21}$$

Equations (18) and (19) can be used to express two of the remaining five quantities by the other three, for instance

$$\frac{u_0}{v_A} = \left(\frac{\eta}{B_0 \Delta}\right)^{1/2} \equiv S_0^{-1/2}, \tag{22}$$

$$\frac{\delta}{\Delta} = S_0^{-1/2}. \tag{23}$$

Equation (22) shows that the reconnection rate is $\partial_t \psi = E = u_0 B_0 \sim \eta^{1/2}$ for macroscopic sheet length $\Delta \sim L$, which is far too slow to explain the time scales observed for instance in a solar flare. To achieve sufficiently fast reconnection current sheets of much smaller length are required, as for instance assumed in Petschek's theory (erroneously, see section 3.6), or as develop in MHD turbulence (Biskamp and Welter, 1989a).

It should be emphasized that current sheets are formed under quite general conditions. Figure 2 gives an example of a dynamic, initially smooth magnetic configuration ψ with four X-points (Fig. 2a), where current sheets develop shrinking in width (Fig. 2b,c), until resistivity becomes important setting up a quasi-stationary Sweet-Parker sheet. The location of current sheets in a general 3D sheared magnetic configuration depends on the structure of the flows as excited for instance by an instability. The presence of a strong axial field $B_z \gg B_\perp$ provides a justification of the incompressibility assumption, which might appear doubtful in the sheet, where the velocity becomes large reaching the Alfvén speed of the reconnected field component $B_\perp$. If the latter is small compared with the axial component, the total Alfvén velocity is still much greater than the flow speed, which guarantees that the perpendicular flow is incompressible.

I should point out that a Sweet-Parker current sheet is also a vorticity sheet, as is clear from the corresponding flow pattern. The vorticity distribution has a quadrupole structure (instead of the monopole structure of the current density), because ω vanishes on the symmetry

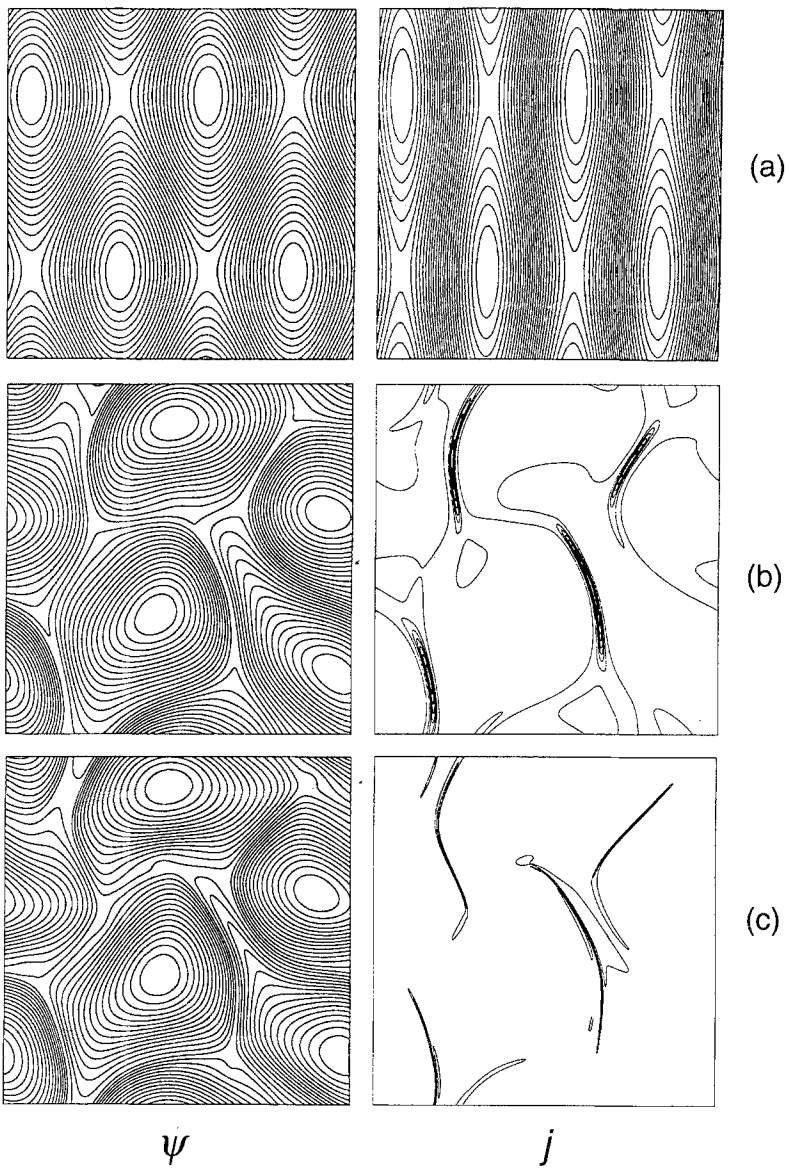

Figure 2. Numerical simulation showing the development of current sheets from a smooth dynamic configuration.

lines of the sheet. Since $u_0 \sim \eta^{1/2} B_0$, the magnitude of the vorticity is, however, small $\omega \sim \eta^{1/2} j$, hence for $\mu \sim \eta$ viscous dissipation $\varepsilon_\mu = \mu \int \omega^2 dV$ is smaller than Ohmic dissipation $\varepsilon_\eta = \eta \int j^2 dV$.

It can be shown by a simple power expansion (Cowley, 1975), that in a Sweet-Parker sheet the magnetic field structure in the vicinity of the neutral point in the sheet center differs basically from a normal

X-point. In particular the separatrix branches do not intersect at a finite angle but osculate as shown in Fig. 3. This result underlines the inherent tendency toward current sheet formation at an X-point.

While the main part of a current sheet configuration is smooth, the outflow or edge regions show a rather complicated quasi-singular behavior. In a seminal paper Syrovatskii (Syrovatskii, 1971) presents a simple theory of current sheets, which appear as branch cuts of a complex potential function. He derives an expression for the sheet current density integrated across the sheet width $J(y)$, where y = the coordinate along the sheet:

$$J(y) = 2\left(\frac{I}{2\pi} + \frac{\Delta^2}{2} - y^2\right) \Big/ \sqrt{\Delta^2 - y^2}. \tag{24}$$

Here I is the total sheet current and Δ the length of the sheet. Expression (24) has the interesting feature that $J(y)$ reverses sign being positive, i.e. in the direction of the total current in the central part $|y| < y_0$, and negative in the outer parts $|y| > y_0$, with $y_0^2 = (I/2\pi) + \Delta^2/2$. At the sheet edges $|y| = \Delta$ the current density becomes singular.

Resistive MHD simulations essentially confirm Syrovatskii's prediction (24). The current density in the sheet is found to reverse sign and to exhibit a quasi-singular structure in the edge regions of the sheet (Biskamp, 1986). The current density changes sign at the position, where the velocity reaches its maximum along the sheet, $v = v_A$. The fluid is subsequently decelerated in the negative current density part and finally completely blocked, turned around and accelerated again along smaller secondary sheets, formed on both sides of the quasi-singular edges of the primary sheet. For still smaller η tertiary sheets become visible, leading to an infinite sequence of higher order sheets in the limit $\eta \to 0$. However, such regular scaling behavior rests on the assumptions of spatial symmetry and stationarity. For more general nonstationary conditions a turbulent state consisting of an irregular ensemble of micro-current sheets is generated (Biskamp and Welter, 1989a), as discussed in section 5.

3.2. Scaling laws for driven resistive reconnection

The concept of driven or forced reconnection plays an important role in reconnection theory. While originally the term referred only to open, externally forced systems in contrast to closed systems, where reconnection occurs spontaneously as an internal process, the concept can be applied much more generally. Assuming that reconnection is localized in space, one may restrict consideration to a subregion L around this location instead of the entire system of size Λ, $L \ll \Lambda$. On the other

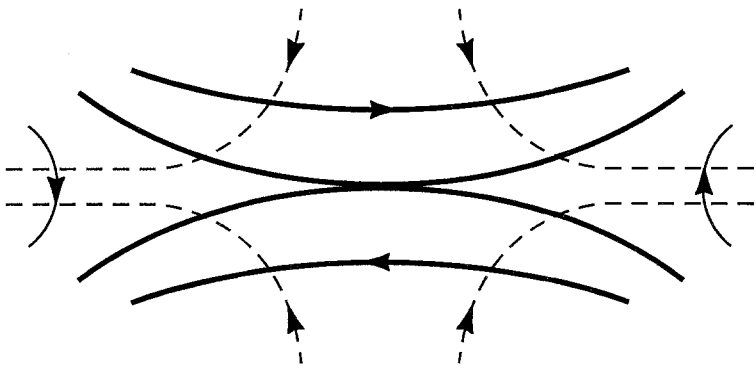

Figure 3. Osculating separatrix branches at the neutral point of a Sweet-Parker sheet.

hand, L should be large compared with the scales of the reconnecting structures, for instance $L \gg \Delta$ in the case of a single current sheet of length Δ, so that these are not affected by the artificial boundaries of the subsystem L. This procedure allows to simplify the geometry and also to assume stationarity even for a nonstationary global system. Since the coupling to the latter occurs through the boundary conditions imposed on the subsystem, which vary on the global time scale Λ/v_A, while the subsystem relaxes on the time scale L/v_A, we may consider the subsystem in steady state (if such a state exists). In this sense the subsystem constitutes a stationary driven reconnection configuration. By assuming up-down and right-left symmetry consideration can be restricted to a quadrant, for instance the upper left quadrant shown in Fig. 4, where the main parameters are indicated. The plasma along with its frozen-in magnetic field is injected from above and after reconnection ejected to the left. While u_∞, B_∞ are given, the internal parameters u_0, B_0 of the current layer and the dimensions δ, Δ are determined by the reconnection process.

A series of simulation runs (Biskamp, 1986) performed for different values of η and the (imposed) reconnection rate E, but identical boundary profile functions yields the following scaling laws of the cur-

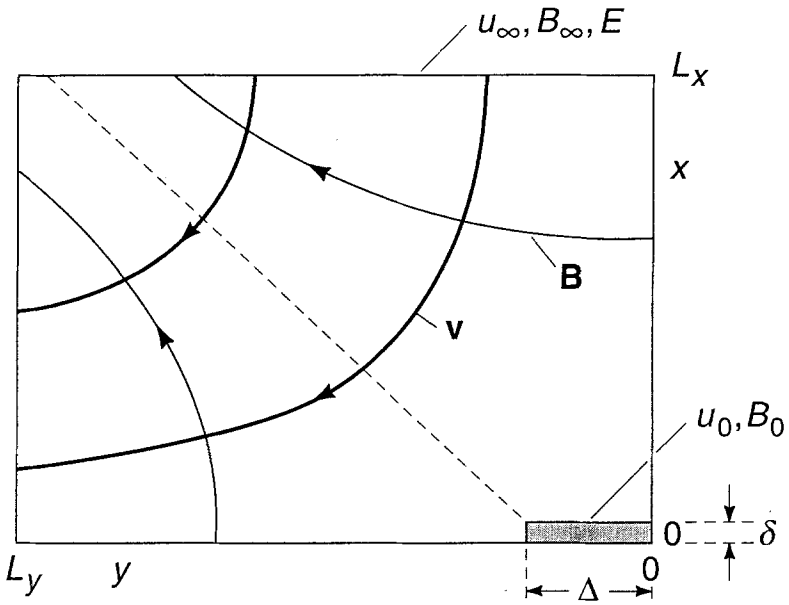

Figure 4. Computational box for driven reconnection studies.

rent sheet parameters

$$B_0 \sim E^2/\eta\,, \tag{25}$$

$$u_0 = E/B_0 \sim \eta/E\,, \tag{26}$$

$$\Delta \sim E^4/\eta^2\,, \tag{27}$$

$$\delta \sim E\eta^0\,. \tag{28}$$

Hence increasing E or decreasing η leads to a rapid stretching of the sheet length Δ as illustrated in Fig. 5. The width δ does not decrease but increases with E contrary to expectation, the reason being the increase (pile-up) of the magnetic field B_0 in front of the layer and the corresponding decrease of u_0, since $u_0 B_0 = E$.

The scaling laws (25) - (28) reflect an important property of the Sweet-Parker sheet. Consider the average inertia force along the sheet. Since the velocity increases about linearly $v_y \simeq B_0 y/\Delta$, we have

$$\overline{v_y \partial_y v_y} \simeq B_0^2/2\Delta \simeq E/2\delta\,, \tag{29}$$

using mass conservation $u_0\Delta = B_0\delta$ and Ohm's law $u_0 B_0 = E$. Hence the scaling (28) implies that the inertia force is invariant to changes of E and η, in particular remains finite for $\eta \to 0$.

When the sheet length Δ reaches the system size L as in Fig. 5c,Δ cannot increase further, and the scaling laws (25)-(28) are no longer

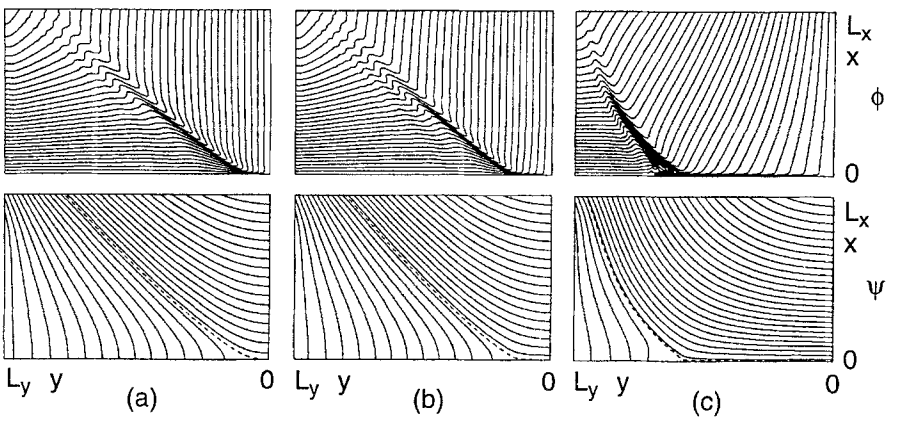

Figure 5. Flux function ψ and stream-function ϕ for three simulation runs with different values of η: (*a*) $\eta = \eta_0$, (*b*) $\eta = \eta_0/2$, (*c*) $\eta = \eta_0/4$, with identical boundary conditions.

valid. Instead we have $\Delta = L$. From $u_0 B_0 = E = \eta B_0/\delta$ one obtains $u_0 = \eta/\delta, B_0 = E\delta/\eta$. Using mass conservation we find

$$B_0 \sim (E^2 L/\eta)^{1/3} , \tag{30}$$

$$\delta \sim (\eta^2 L/E)^{1/3} . \tag{31}$$

In a closed system only a finite amount of free energy is available, hence B_0 is limited. This leads us back to the original sheet relations (22), (23) indicating $u_0 \sim \delta \sim \eta^{1/2}$.

3.3. Petschek's quasi-ideal reconnection model

For two decades Petschek's slow-shock model (Petschek, 1964) was the generally accepted theory of magnetic reconnection. In recent years it has, however, been realized, that the model is not valid in the usually adopted framework of resistive MHD in the limit of small resistivity. Petschek's configuration, illustrated in Fig. 6, is characterized by two pairs of slow shocks standing back to back against the upstream flow, which they deviate by roughly 90^o into the downstream cone between the shocks. Current density and vorticity are concentrated in the shocks and the central current sheet. The shocks derive their properties from

the slow magnetosonic wave, a compressible mode, which survives with finite phase velocity in the incompressible limit, $\omega^2 = k_{||}^2 v_A^2 = k^2 B_n^2$, where B_n is the component normal to the wave front. Hence the flow can be supersonic with respect to this mode for any given speed, if the angle between wave front and magnetic field is sufficiently small.

Petschek's configuration is a solution of the ideal MHD equations valid outside the singularities. The jump conditions at the shocks determine the position of the latter, i.e. the downstream angle α in terms of the upstream velocity. The reconnection rate is essentially independent of the resistivity, which has been the most attractive feature of the model. The ideal solution must, however, be matched to the resistive solution in the current sheet, which is very difficult and has previously been essentially ignored. Petschek *assumes* a current sheet of dimensions $\Delta \sim \delta \sim \eta$ adjusting automatically to the external solution. This is, however, not true. Numerical solutions of the full resistive problem show that Δ does not shrink with η, but becomes macroscopically large following the scaling laws (25)-(28), which changes the external configuration fundamentally and leads to a slow Sweet-Parker type reconnection rate $E = O(\eta^{1/2})$. Petschek's model may, however, be applicable, if the conditions in the reconnection region are alleviated. This is achieved by a locally enhanced effective resistivity $\eta_{eff} = O(1)$ due to turbulence generated for instance by the high current density in the sheet (Sato and Hayashi, 1979). Macroscopic current sheet formation can also be avoided, if collisionless reconnection processes are dominant as discussed in section 6.

4. Paradigms of resistive reconnection

The natural configuration of a magnetized plasma in the absence of nearby boundary surfaces or other types of forcing is a circular plasma tube or pinch (Fig. 7a), for instance a coronal loop. External forces may change this configuration primarily in two ways, either by stretching into an elongated sheet-like state (Fig. 7b) as in the case of the solar wind stretching the earth dipole field into the magnetotail configuration, or by twisting (Fig. 7c) such as performed by photospheric convection on coronal loops. Both processes lead to energization of the configuration, which gives rise to relaxation processes, if certain thresholds are exceeded. The stretched configuration becomes unstable to the tearing mode breaking up into several plasma tubes (Fig. 7d), which then coalesce into a single tube. In the twisted case the plasma tube kinks into a helical configuration (Fig. 7e), which is then carried back into a less twisted straight tube by the resistive kink mode.

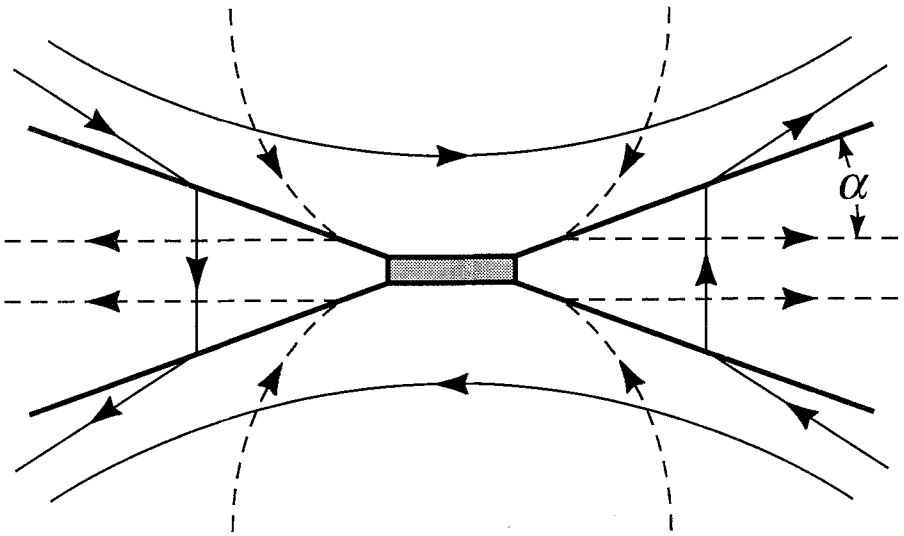

Figure 6. Schematic drawing of Petschek's slow-shock configuration.

The basic mechanism driving these relaxation processes is the attractive force between parallel currents. Tearing, coalescence and (resistive) kinking involve large-scale reconnection, which I will consider more in detail in the following. We should of course keep in mind that the sequence of events sketched in Fig. 7 is highly idealized ignoring 3D effects, for instance two flux tubes in general encounter obliquely under a finite angle. Nevertheless, these processes play a fundamental role in analyzing and understanding nonlinear plasma dynamics, serving as paradigms of reconnecting systems.

4.1. The tearing instability

The tearing mode is probably the most frequently invoked instability in the context of magnetic reconnection. Nevertheless, its peculiar properties, in particular the slow nonlinear evolution, do not seem to be well known. I first recapitulate briefly the linear theory (Furth et al., 1963). Consider a plane configuration $\mathbf{B}_0 = (0, B_{0y}(x), B_{0z}(x))$, where the poloidal field reverses sign at $x = 0$, so that in the vicinity of this surface $B_{0y}(x) \simeq B'_{0y}x = \psi''_0 x$. In the presence of a sinusoidal perturbation one has

$$\psi(x,y) = \psi''_0 x^2/2 + \psi_1(x,t)\cos ky, \tag{32}$$

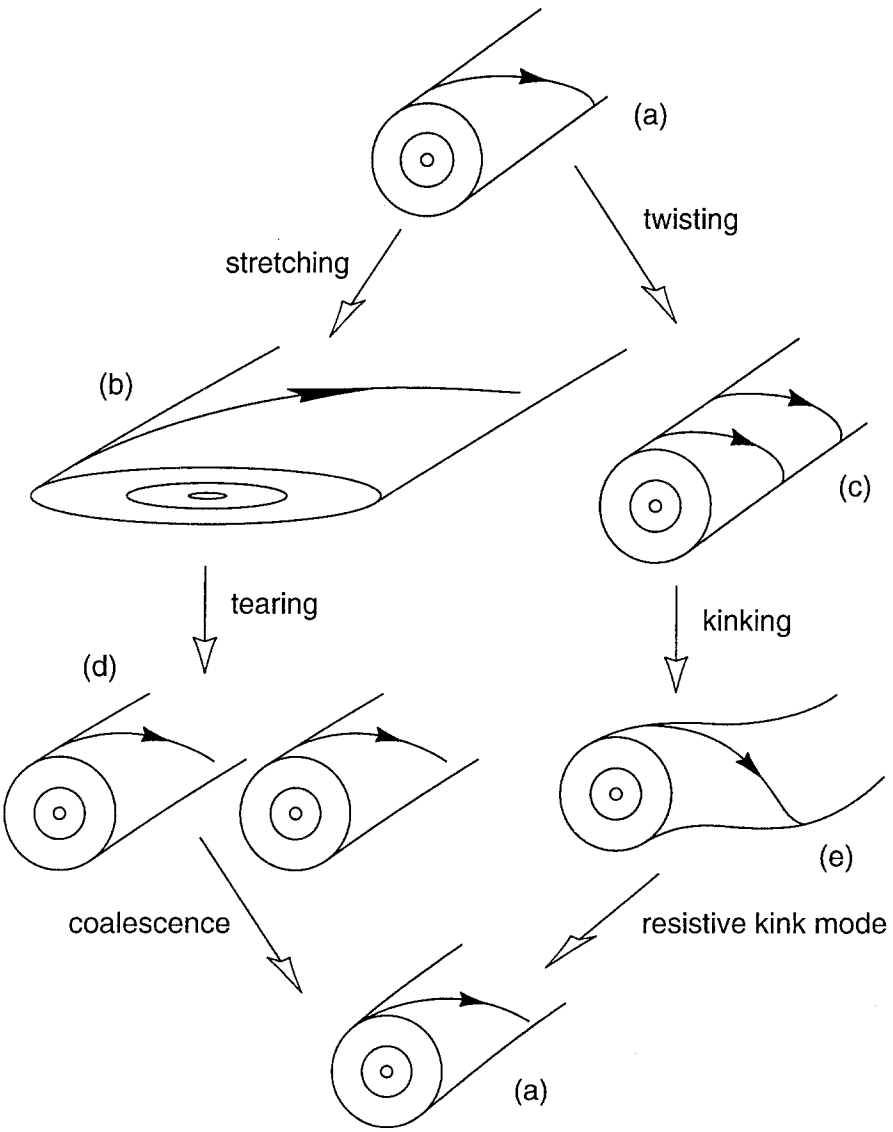

Figure 7. A circular pinch, forced externally, tends to relax back into a circular shape by different reconnection processes.

which consists of an alternating sequence of X- and O-points. The perturbation is characterized geometrically by the island size w, the distance between the separatrix branches at the O-point,

$$w = 4\sqrt{\psi_1/\psi_0''}, \tag{33}$$

ignoring the x-dependence of ψ_1. Linearizing eqs. (16), (17) and neglecting the viscous term one obtains

$$\partial_t \nabla^2 \phi_1 - \mathbf{B}_0 \cdot \nabla j_1 - \mathbf{B}_1 \cdot \nabla j_0 = 0 \ , \tag{34}$$

$$\partial_t \psi_1 - \mathbf{B}_0 \cdot \nabla \phi_1 = \eta \nabla^2 \psi_1 \ , \tag{35}$$

where for eigenmodes $\psi_1, \phi_1 \propto e^{\gamma t}$. Since the highest order derivative in eq. (35) is multiplied by the small parameter η, we have to solve a boundary layer problem. We distinguish between the narrow resistive layer, where $B_{0y} \simeq 0$, such that in eq. (35) the resistive term is important, and the external region, where B_{0y} is finite. In the resistive layer, $\mathbf{B}_0 \cdot \nabla = ikB_{0y} = ixF$ with $F = kB'_{0y}$, and $\nabla^2 \simeq \partial_x^2$, such that eqs. (34), (35) become (index i for "inner" solution)

$$\gamma \phi_i'' = ixF\psi_i'' \ , \tag{36}$$

$$\gamma \psi_i = ixF\phi_i + \eta \psi_i'' \ . \tag{37}$$

In addition we assume that $\psi_i(0)$ is finite, hence $\psi_i = \text{const.}$ inside the narrow layer, which is called the constant-ψ approximation. With

$$\psi_i'' \simeq \Delta_i' \frac{\psi_i}{\delta} \ , \ \phi_i'' \simeq \frac{\phi_i}{\delta^2} \, , \tag{38}$$

where δ is the layer width and Δ_i' is the change of ψ_i' across the layer,

$$\Delta_i' = [\psi_i'(\delta) - \psi_i'(-\delta)]/\psi_i \, , \tag{39}$$

we can evaluate eqs. (36), (37) approximately

$$\gamma \simeq \eta^{3/5} (\Delta'_i)^{4/5} F^{2/5} \, , \tag{40}$$

$$\delta \simeq \eta^{2/5} (\Delta'_i)^{1/5} F^{-2/5} \ . \tag{41}$$

One can show that instability arises, i.e. $\gamma > 0$, if $\Delta_i' > 0$. We can also see that the constant-ψ approximation is in fact valid, by comparing the time $\tau_\delta = \delta^2/\eta \sim \eta^{-1/5}$ for a magnetic perturbation to diffuse across the layer (and hence assume a finite value $\psi_i(0)$) with the growth time $\gamma^{-1} \sim \eta^{-3/5}$, $\tau_\delta \ll \gamma^{-1}$.

In the external region, where B_{0y} is finite, not only the resistive term in eq. (35) but also the inertia term in eq. (34) can be neglected, while leaves us with the linearized equilibrium equation,

$$\psi_e'' - \left[k^2 + \frac{j_0'(x)}{B_{0y}(x)}\right]\psi_e = 0 \tag{42}$$

In general the external solution $\psi_e(x)$ is not smooth at $x = 0$. By asymptotically matching the layer solution to the external one, we identify Δ_i' in eq. (40) with the jump Δ_e' of the derivative of the external solution at $x = 0$

$$\Delta_i' = \Delta_e' = [\psi_e'(0_+) - \psi_e'(0_-)]/\psi_e(0) = \Delta' \,, \tag{43}$$

which determines the growth rate γ. In general $\Delta' > 0$ for $ka < 1$, where a is the gradient scale of the current profile $j_0(x)$.

With $\gamma \sim \eta^{3/5}$ the tearing mode has the appearance of a relatively fast reconnection process, not much different from the Sweet-Parker scaling $\eta^{1/2}$, which is in fact reached for the maximum growth rate at $ka \sim \eta^{-1/4}$. The exponential growth is, however, nonlinearly slowed down already at microscopic island width $w \sim \delta$. The main nonlinear effect is the flattening of the current profile $j_0(x)$ over the island width, which implies that in the linear equation (37) δ is to be replaced by w

$$\partial_t \psi_i \simeq \eta \frac{\Delta'}{\delta}\psi_i \;\rightarrow\; \eta \frac{\Delta'}{w}\psi_i \quad \text{for } w > \delta \,.$$

Hence the nonlinear growth is slow (Rutherford, 1973)

$$w \simeq \eta \Delta' t \tag{44}$$

corresponding to a reconnection rate $E \sim \eta$, which is consistent with the absence of a macroscopic current sheet. This result is, however, strictly valid only in a periodic, i.e. closed configuration. The tearing mode in a Sweet-Parker sheet of finite length develops on a faster time scale, see section 4.4.

4.2. Resistive kink instability

The kink instability is the most fundamental MHD instability in a plasma column, which occurs if the twist of the magnetic field exceeds a threshold given by $B_p L / B_z a > 2\pi$, where L is the length and a the radius of the column. The kink mode corresponds to a rigid helical shift of the column pushing against the surrounding plasma and magnetic

field, which generates a current sheet at the so-called resonant surface $r = r_s$, where $B_p L/B_z r_s = 2\pi$. In its simplest form the resistive kink instability can be discussed in the same framework as the tearing mode in section 4.1. In the narrow layer around r_s eqs. (36), (37) apply with $x = r - r_s$, but since the instability is much faster, the constant-ψ approximation does not hold, such that $\psi_i'' \sim \psi_i/\delta^2$. One thus obtains

$$\gamma \simeq \eta^{1/3} F^{2/3}, \delta \simeq \eta^{1/3} F^{-2/3}. \tag{45}$$

Hence γ is larger than for the tearing mode, eq.(40). Nonlinearly the evolution of the resistive kink instability is determined by the reconnection in a current sheet of macroscopic length (Waelbroeck, 1989; Biskamp, 1991).

Conventionally, the kink mode is studied in a periodic system, practically speaking a toroidal plasma column, since primary interest in MHD instabilities has been for application in laboratory plasmas in fusion research. In twisted coronal loops with line-tying in the photosphere the kink mode does not develop as a uniform helical displacement, but is rather localized in the central part along the column, and so is the reconnection region (Amo et al., 1995). Because of this localization the reconnection process associated with the kink mode can be more rapid than in the periodic case.

4.3. Coalescence of magnetic flux bundles

The most instructive example of fast reconnection is the coalescence of two flux bundles, for instance of two magnetic islands generated by the tearing mode. Consider for instance the corrugated sheet pinch equilibrium (Fadeev et al., 1965)

$$\psi(x,y) = B_\infty a \ln(\cosh\frac{y}{a} + \varepsilon\cos\frac{x}{a}), \tag{46}$$

which consists of a periodic chain of magnetic islands around the midplane $y = 0$ imbedded in an antiparallel field $B_x \to \pm B_\infty$ for $y \to \pm\infty$. The island width w is given by the parameter ε, $w/a \simeq 4\sqrt{\varepsilon}$ for $w \ll a$. The configuration (46) is unstable to pairwise attraction and coalescence of islands for any island width (Pritchett and Wu, 1979). The nonlinear process, which has been studied numerically (see, e.g. Biskamp and Welter, 1980) consists of an ideal MHD phase, where the islands are freely accelerated toward each other, which leads to flux compression and current sheet formation, and a slower reconnection phase. For intermediate values of η, a self-similar behavior is observed, with the scaling laws for the upstream quantities u_0, B_0, i.e. v_x and B_y taken in front of

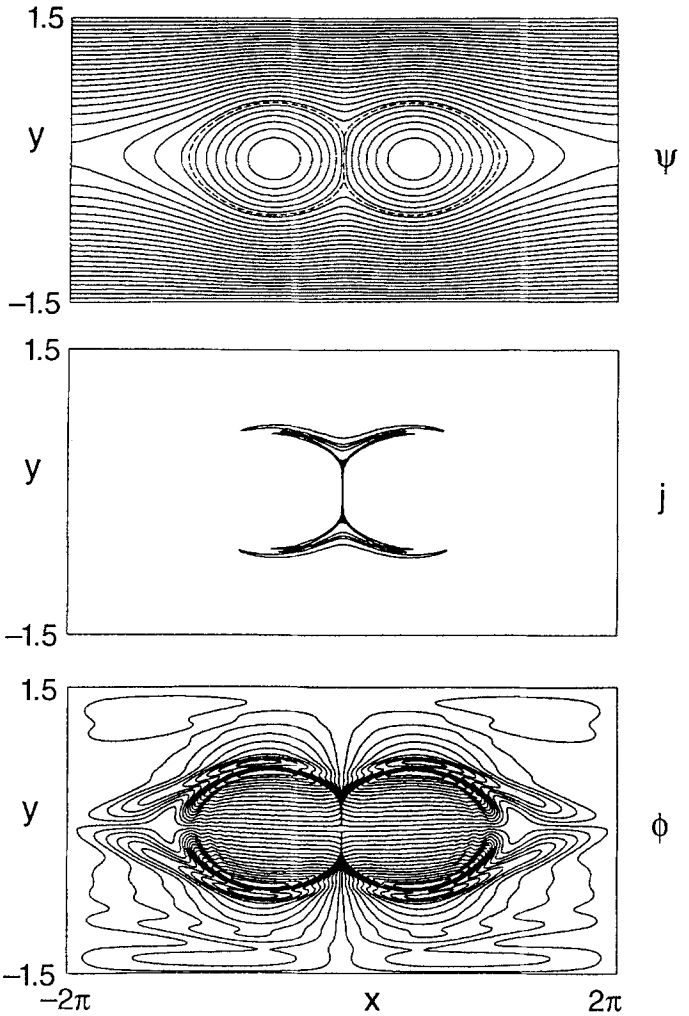

Figure 8. Coalescence of two magnetic islands starting from the equilibrium eq. (46).

the current sheet between the two islands, $u_0 \sim \eta^{1/3}, B_0 \sim \eta^{-1/3}$. As a consequence the reconnection rate $E = u_0 B_0$ is independent of η, which corresponds to the scaling laws (30), (31) for driven reconnection.

As mentioned in section 3.2, in a closed system such a behavior can only be valid for a certain η-range, since B_0 cannot exceed the maximum value B_m which would be obtained in the ideal case $\eta = 0$, when the attractive motion is reversed because of the repelling force due to field compression. Hence the scaling $B_0 \sim \eta^{-1/3}$ breaks down for $B_0 \simeq B_m$. For smaller values of η one finds a Sweet-Parker scaling $u_0 \sim \eta^{1/2}, B \simeq B_m$. The behavior during the coalescence is illustrated in Fig.

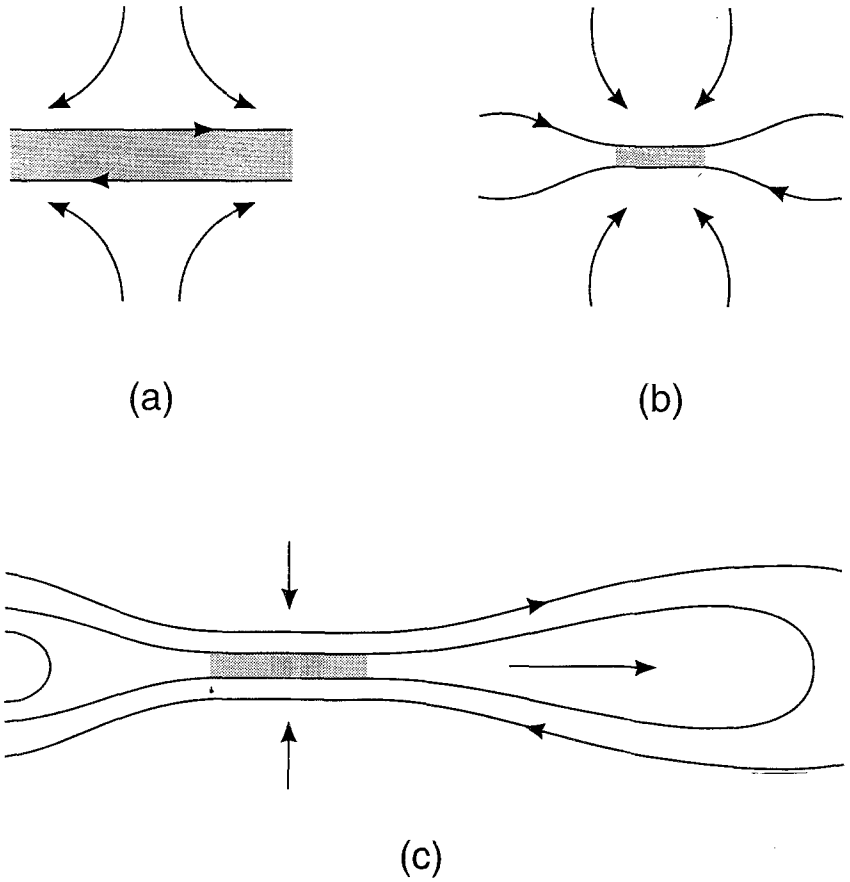

Figure 9. Local thinning of a current sheet leads to faster reconnection (b) and plasmoid generation (c).

8. The current sheet exhibits all the characteristic features discussed in section 3.1.

These coalescence simulation as well as simulations of the nonlinear resistive kink instability prove (or at least give strong evidence) that the results of driven reconnection given in section 3.2 are representative of the behavior of resistive reconnection and that contrary to the basic assumption implied in Petschek's model, resistive reconnection takes place in macroscopic current sheets, as long as these are stable and a stationary configuration exists.

4.4. Tearing instability of a Sweet-Parker sheet and the generation of plasmoids

In a static sheet pinch, for which the tearing mode is usually considered, the instability condition $ka < 1$ (see section 4.1) implies that a sheet pinch of length Δ and width δ becomes unstable, if it accommodates more than, say, two marginally unstable wavelengths, $\Delta/\delta \simeq 2\lambda_c/\delta \sim 10$, $\lambda_c = 2\pi/k_c = 2\pi\delta$. The existence of apparently stable sheets of much larger Δ/δ as observed in numerical simulations indicates that in a Sweet-Parker sheet the strong inhomogeneous flow has a stabilizing effect (Bulanov et al., 1979; Syrovatskii, 1981). The velocity increases linearly along the sheet, $v_y(y) = \Gamma y$, where $\Gamma = v_A/\Delta = u/\delta = \eta/\delta^2$ using the properties of a Sweet-Parker sheet. The stability condition is roughly $\Gamma \simeq \gamma$, where γ is the tearing mode growth rate for a static configurationdiscussed in section 4.1. This result can easily be understood. While the tearing instability corresponds to a local current density condensation, the inhomogeneous flow tends to pull such current blobs apart. Hence the tearing mode can only be unstable, if the inhomogeneity is sufficiently weak. More quantitatively, the mode is stabilized, if the relative increase of the wavelength $\Delta\lambda/\lambda$ during one growth time exceeds about $1/4$

$$\left(v_y(y+\lambda) - v_y(y)\right)/\gamma_{max}\lambda = \Gamma/\gamma_{max} > \frac{1}{4}. \tag{47}$$

Inserting the maximum growth rate $\gamma_{max} \propto \eta^{1/2}$ gives a condition for the maximum stable current sheet length. Tearing instability can hence be expected for

$$\Delta/\delta \gtrsim 10^2. \tag{48}$$

The nonlinear dynamics of the tearing mode in a current sheet is in general quite different from that in a closed periodic configuration. Instead of a chain of magnetic islands typically only one island, a so-called plasmoid, is generated in the central part of the sheet, which is then convected along the sheet while still growing self-similarly in size. The basic instability mechanism is a local thinning of the current sheet, as illustrated in Fig. 9. While in the unperturbed sheet flux is piled up slowing down of the upstream flow (diverging flow pattern, Fig. 9a), a local thinning leads to field expansion and flow acceleration (converging flow, Fig. 9b), which increases the reconnection efficiency by reducing the local Lundquist number S_0, eq. (22). Note that both the field B_0 and the sheet length Δ in S_0 are reduced.

Contrary to the tearing mode in a periodic system the plasmoid growth and ejection is a nonequilibrium process. As illustrated in Fig. 9c

the plasmoid is pushed away from the reconnection point by an imbalance of forces, which gives rise to a fast quasi-Alfvénic motion along the sheet. Reconnection occurs in a macroscopic current sheet and is much faster, $E \sim \eta^{1/2}$, than in the periodic nonlinear tearing mode with $E \sim \eta$, since the reconnected flux is carried away with the plasmoid pulling new flux from above and below into the reconnected region. Since plasmoid ejection takes place on the Alfvén time scale τ_A, while the supply of reconnected flux is much slower $\eta^{1/2}\tau_A$, the plasmoids tend to be rather narrow. For sufficiently small η the current sheet itself becomes unstable, giving rise to secondary plasmoids.

Plasmoids are believed to be important in various kinds of eruptive processes, notably in magnetospheric substorms and two-ribbon flares (Mikic et al., 1988; Biskamp and Welter, 1989b). Figure 10 gives a sequence of plasmoid states from a 2D compressible MHD simulation of the magnetotail (Hautz and Scholer, 1987). A large anomalous resistivity is assumed at the primary X-point at $x = 2.5$, which leads to large plasmoids. The first plasmoid is accelerated along the sheet in the direction of decreasing field intensity and pressure away from the earth (Fig. 10a). A long thin current sheet is generated between the dipole field on the left and the plasmoid (Fig. 10b), which becomes unstable generating a secondary plasmoid (Fig. 10c), which catches up and finally coalesces with the first large one (Fig. 10d). Interaction with the downtail plasma, which is still at rest, leads to shock formation and a blunt leading edge, giving the plasmoid a drop-like shape. Three-dimensional effects do not change the general picture (Birn and Hones, 1981; Otto et al., 1990). Kageyama et al. (1990) present global simulations of the interaction of the solar wind with the magnetosphere. A long tail is formed giving rise to continuous generation of plasmoids. It should, however, be mentioned that the basic problem in the theory of magnetospheric substorms is the identification of the reconnection mechanism, i.e. the relevant effect in Ohm's law, which has to be a primarily nondissipative process, since the magnetotail plasma is collisionless. I will discuss such processes in section 6. In addition, as in all eruptive processes, the problem of onset conditions arises, i.e. why is the configuration suddenly erupting after a long quiescent period.

5. MHD turbulence

A fundamental issue in magnetic reconnection theory is to explain the fast observed time scales, which for typical eruptive events, in particular in astrophysics, seem to be essentially independent of the value of the

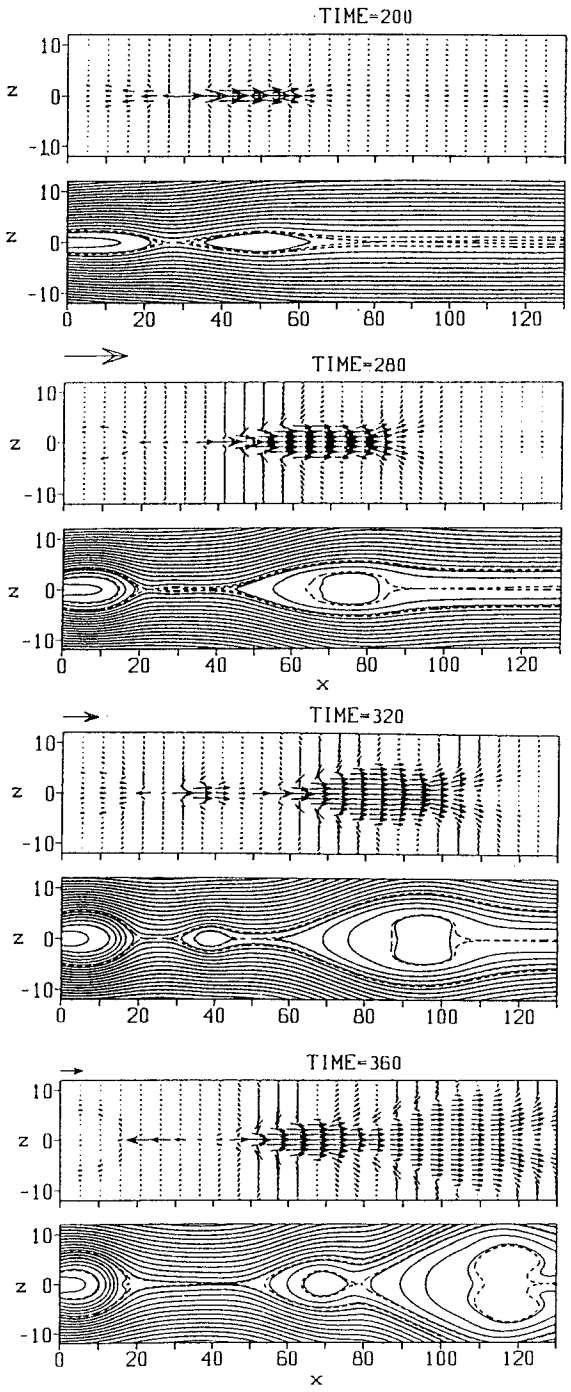

Figure 10. Compressible MHD simulation of plasmoid generation in the earth's magnetotail (from Hautz and Scholer, 1987).

collisional resistivity. As a consequence stationary current sheet reconnection, which appears to be the dominant mechanism at intermediate R_m, are far too slow at almost collisionless plasma conditions, where R_m is formally very large. It will be discussed in section 6 that under such conditions nondissipative effects in Ohm's law are important. However, also in the framework of resistive MHD fast η-independent reconnection is possible by a strongly nonstationary behavior in the reconnection region. A first indication of such behavior has been given in the previous section, the tearing instability of the Sweet-Parker sheet leading the plasmoid generation and ejection. It is not difficult to visualize the transition to fully developed MHD turbulence for still larger R_m and less symmetric systems. In this section I summarize the most important properties of MHD turbulence (for more details see Biskamp, 1993).

5.1. Global and spectral properties

While nonmagnetic hydrodynamic turbulence is characterized by a single dimensionless parameter, the Reynolds number $Re = vL/\mu$, there are two in the MHD case, Re and R_m, or R_m and the magnetic Prandtl number $Pr_m = \mu/\eta$. Since for $Pr_m \lesssim 1$ the dependence on Pr_m is weak, most studies of MHD turbulence assume $Pr_m = 1$, excluding the viscosity dominated regime $Pr_m \gg 1$.

The evolution of turbulence is strongly influenced by the ideal invariants of the system. For incompressible MHD, eqs. (13), (14), there are three invariants, the total energy W, the cross-helicity K, and the magnetic helicity H^A, defined by

$$W = W^V + W^M = \tfrac{1}{2}\int (v^2 + B^2) d^3x\,, \tag{49}$$

$$K = \tfrac{1}{2}\int \mathbf{v}\cdot\mathbf{B}\; d^3x\,, \tag{50}$$

$$H^A = \tfrac{1}{2}\int \mathbf{A}\cdot\mathbf{B}\; d^3x\,, \tag{51}$$

where $\mathbf{A}$ is the vector potential, $\nabla\times\mathbf{A} = \mathbf{B}$. In 2D there are also three (quadratic) invariants, the first two, W and K, are formally identical with the 3D expressions, while H^A is replaced in 2D by the mean square magnetic potential

$$H^\psi = \tfrac{1}{2}\int \psi^2 d^2x\,. \tag{52}$$

Including finite dissipation coefficients η, μ these invariants are in general found to decay in magnitude, but the decay rates $\Gamma^W = (dW/dt)/W$

etc., with

$$dW/dt = -\eta \int j^2 d^3x - \mu \int \omega^2 d^3x\,, \tag{53}$$

$$dK/dt = -(\eta + \mu) \int \boldsymbol{\omega} \cdot \mathbf{j}\; d^3x\,, \tag{54}$$

$$dH^A/dt = -\eta \int \mathbf{j} \cdot \mathbf{B}\; d^3x, \text{ or } dH^\psi/dt = -\eta \int B^2 d^2x\;, \tag{55}$$

may be general largely different, in particular

$$\Gamma^W \gg \Gamma^A, \text{ or } \Gamma^W \gg \Gamma^\psi \text{ in 2D}\,, \tag{56}$$

and

$$\Gamma^W \gg \Gamma^K. \tag{57}$$

The different magnitudes of in the Γ's, called selective decay (Matthaeus and Montgomery, 1980) arise, because the strongest dissipation occurs at small scales and dW/dt contains higher derivatives than $dH^{A,\psi}/dt$, and because the integrand in dW/dt is positiv, while its sign varies in dK/dt leading to cancellations. The existence of several ideal invariants and their selective decays result in self-organization processes in decaying turbulence. On intermediate time scales $(\Gamma^W)^{-1} \ll t \ll (\Gamma^A)^{-1}$, or $(\Gamma^W)^{-1} \ll t \ll (\Gamma^\psi)^{-1}$ in 2D, the system relaxes to a state of minimum energy for a given value of H^A or H^ψ, which can be formalized by the variational principle

$$\delta \left[\int (v^2 + B^2) d^3x - \lambda \int \mathbf{A} \cdot \mathbf{B} d^3x \right] = 0\;, \tag{58}$$

the result of which is a static linear force-free field (Woltjer, 1958; Taylor, 1986)

$$\nabla \times \mathbf{B} - \lambda \mathbf{B} = 0\;,\; \mathbf{v} = 0\;, \tag{59}$$

and in 2D

$$\delta \left[\int (v^2 + B^2) d^2x - \lambda^2 \int \psi^2 d^2x \right] = 0 \tag{60}$$

with a similar linear field solution

$$\nabla^2 \psi + \lambda^2 \psi = 0\;,\; \nabla^2 \phi = 0. \tag{61}$$

Hence both in 3D and 2D the system relaxes to a static state $W^V/W^M \to 0$. The origin of this asymmetry between $\mathbf{B}$ and $\mathbf{v}$ is the lack of a conserved kinetic quantity equivalent to the magnetic ones H^A or H^ψ. The selective decay (57) leads to a different self-organization process,

the alignment of $\mathbf{v}$ and $\mathbf{B}$ called dynamic alignment (Matthaeus and Montgomery, 1984). The appropriate variational principle

$$\delta\left[\tfrac{1}{2}\int(v^2+B^2)d^3x-\lambda\int\mathbf{v}\cdot\mathbf{B}d^3x\right]=0. \tag{62}$$

has the solutions (both in 3D and 2D)

$$\mathbf{v}=\pm\mathbf{B}\ , \tag{63}$$

which are called pure Alfvénic states. A dynamic mechanism of this relaxation has been developed by Dobrowolny et al. (1980). Strongly aligned states are often observed in the solar wind (e.g. Burlage and Turner, 1976). Which of the two relaxation processes dominates, the formation of force-free states (which in 3D is in alignment of $\mathbf{j}$ and $\mathbf{B}$) or the dynamic alignment of $\mathbf{v}$ and $\mathbf{B}$, depends on the initial values of H^A (or H^ψ) and K.

Quadratic ideal invariants are connected with detailed balance relations in wavenumber space meaning that the corresponding spectral quantities, e.g. $W_\mathbf{k}$, are conserved in elementary interactions between any triad of modes $\mathbf{k},\mathbf{p},\mathbf{q}$ with $\mathbf{k}+\mathbf{p}+\mathbf{q}=0$, $W_\mathbf{k}+W_\mathbf{p}+W_\mathbf{q}=\text{const.}$ If such a quantity is injected into a certain spectral range $k\sim k_{in}$, it will diffuse in k-space. If this flow is primarily to large k, the quantity is said to exhibit a normal or direct cascade, and an inverse cascade, if the flow is to small k. Turbulence can be characterized by the cascade directions of its ideal invariants. Table 1 gives the cascade directions in MHD turbulence in 3D and 2D compared with the corresponding ones in Navier-Stokes turbulence, where in the latter W_k refers to the kinetic energy, H_k to the kinetic helicity, and Ω_k to the mean square vorticity. While the cascade properties in Navier-Stokes turbulence differ fundamentally in 3D and 2D, they are essentially identical for MHD turbulence indicating a stronger similarity between 3D and 2D than in the Navier-Stokes case. The presence of several ideal invariants with different cascade directions is generally believed to give rise to large-scale self-organization, i.e. the formation of large-scale coherent structures. In 2D Navier-Stokes turbulence these are large-scale velocity eddies (generated by isolated vortices), while in MHD turbulence these are large-scale magnetic structures.

In addition to the local mode interactions giving rise to the cascade flows MHD turbulence also exhibits nonlocal interactions in k-space corresponding to large scales directly affecting small scales, which is absent in Navier-Stokes turbulence. The magnetic field in the large-scale eddies containing most of the magnetic energy acts as a guide field $\mathbf{B}_0$ to the small-scale fluctuations $\tilde{\mathbf{B}},\tilde{\mathbf{v}}$, which thus become strongly

Table I. Cascade directions in 3D and 2D for MHD and Navier-Stokes turbulence.

	3D		2D	
MHD	W_k	direct	W_k	direct
	K_k	direct	K_k	direct
	H_k^A	inverse	H_k^ψ	inverse
Navier-Stokes	W_k	direct	W_k	inverse
	H_k	direct	Ω_k	direct

correlated,

$$\tilde{\mathbf{v}} \simeq \pm\tilde{\mathbf{B}} \,, \tag{64}$$

propagating as Alfvén waves along $\mathbf{B}_0$. (Note the difference between a global alignment eq. (63), which occurs only in a relaxed state, and the small-scale property (64), which is satisfied under normal turbulence conditions). The basic effect of (64) on the turbulent dynamics becomes evident, if we rewrite the MHD equations in terms of the Elsässer fields $\mathbf{z}^\pm = \mathbf{v} \pm \mathbf{B}$ (Elsässer, 1950)

$$\partial_t \mathbf{z}^\pm \mp \mathbf{v}_A \cdot \nabla \mathbf{z}^\pm + \mathbf{z}^\mp \cdot \nabla \mathbf{z}^\pm = \text{pressure and dissipation terms}\,, \tag{65}$$

where we have split off the large-scale field $\mathbf{B}_0 = \mathbf{v}_A$ to emphasize the Alfvén wave propagation properties. The crucial effect is that only waves propagating in opposite directions couple. Hence the interaction time between two eddies is $\tau \sim \tau_A = (kv_A)^{-1}$, which is short compared with the nonlinear scrambling time of hydrodynamic eddies $\tau \sim (k\tilde{v})^{-1}$, since $\tilde{v} \sim \tilde{B} \ll B_0$. This is called the Alfvén effect in MHD turbulence (Iroshnikov, 1964; Kraichnan, 1965), which strongly affects the energy transfer in the turbulent cascade process.

A characteristic property of high Reynolds-number turbulence is the existence of an inertial range in the energy spectrum defined by $k_{in} \ll k \ll k_d$, where k_{in} is the injection range, corresponding to the large energy-containing scales, and k_d is the dissipation range, the smallest scales excited. The angle-integrated energy spectrum W_k, $W = \int W_k dk$, can be "derived" by dimensional arguments. Assuming that the energy transfer rate ε, which is constant in the inertial range and equal to the energy dissipation rate, is only a function of k, W_k, v_A, and that due to the Alfvén effect $\varepsilon \propto \tau_A$, one obtains $\varepsilon \sim v_A^{-1} W_k^2 k^3$, or

$$W_k \sim (\varepsilon v_A)^{1/2} k^{-3/2} \,, \tag{66}$$

which is less steep than the well-known Kolmogorov law for hydrodynamic turbulence $W_k \sim \varepsilon^{2/3} k^{-5/3}$. The MHD spectrum (66) should

apply to both 3D and 2D (in contrast to the Kolmogorov law, which is only valid in the 3D hydrodynamic case). In fact the spectrum (66) has been verified in 2D simulations (Biskamp and Welter, 1989a). The only high-R_m system of MHD turbulence, where the energy spectrum has been measured, is the solar wind. Here the spectral index appears to be close to 5/3 (e.g. Matthaeus et al., 1982), from which it has been concluded that in the solar wind the energy spectrum follows the Kolmogorov law instead of the flatter spectrum (66). However, only the magnetic part of the energy spectrum is measured, which in a refined theory is predicted to be somewhat steeper than $k^{-3/2}$, since $W_k^M - W_k^V = ak^{-2} > 0$ (Grappin et al., 1983).

Spectral laws can also be obtained for inversely cascading quantities in the range $k < k_{in}$. Assuming a constant magnetic helicity flux η_H one obtains the helicity spectrum $H_k^A \sim \eta_H^{2/3} k^{-2}$, and correspondingly in 2D $H_k^\psi \sim \eta_\psi^{2/3} k^{-7/3}$ for a constant mean square potential flux η_ψ. The latter law has been verified in numerical simulations (Biskamp and Bremer, 1994).

5.2. Turbulent energy dissipation

In a magnetic configuration with a macro-current sheet the energy dissipation rate (53) is small, $\varepsilon = O(\eta^{1/2})$, as follows from the properties of a Sweet-Parker sheet. Since for sufficiently high R_m the system becomes turbulent, the question arises, whether the turbulent energy dissipation rate remains finite in the limit $R_m \to \infty$. This behavior is generally believed to be valid for Navier-Stokes turbulence, where a decrease of the viscosity simply leads to the excitation of smaller scales such that ε is essentially independent of μ. (This is, however, not true in the 2D Navier-Stokes case, where the energy dissipation is weak, $\varepsilon = O(\mu)$). In MHD turbulence the cascade and spectral properties are very similar in 2D and 3D, as discussed in the previous section. Numerical simulations of decaying 2D MHD turbulence have been performed for different Reynolds numbers (e.g. Biskamp and Welter, 1989a). Dissipation is found to be concentrated in micro-current sheets, distributed intermittently as seen in Fig. 11. Increasing R_m these micro-sheets become both smaller and more numerous , while the macro-state remains essentially unchanged. Quantitatively Fig. 12 gives the evolution of the energy dissipation rate $\varepsilon(t)$ for three cases starting from the same smooth initial conditions but with different values of $(\eta = \mu)$. While in the initial nonturbulent phase $\varepsilon \propto \eta$, in the subsequent phase of fully developed turbulence $(t \gtrsim 1)\,\varepsilon$ is statistically identical in all three cases, i.e. ε is essentially independent of R_m. Such behavior is a

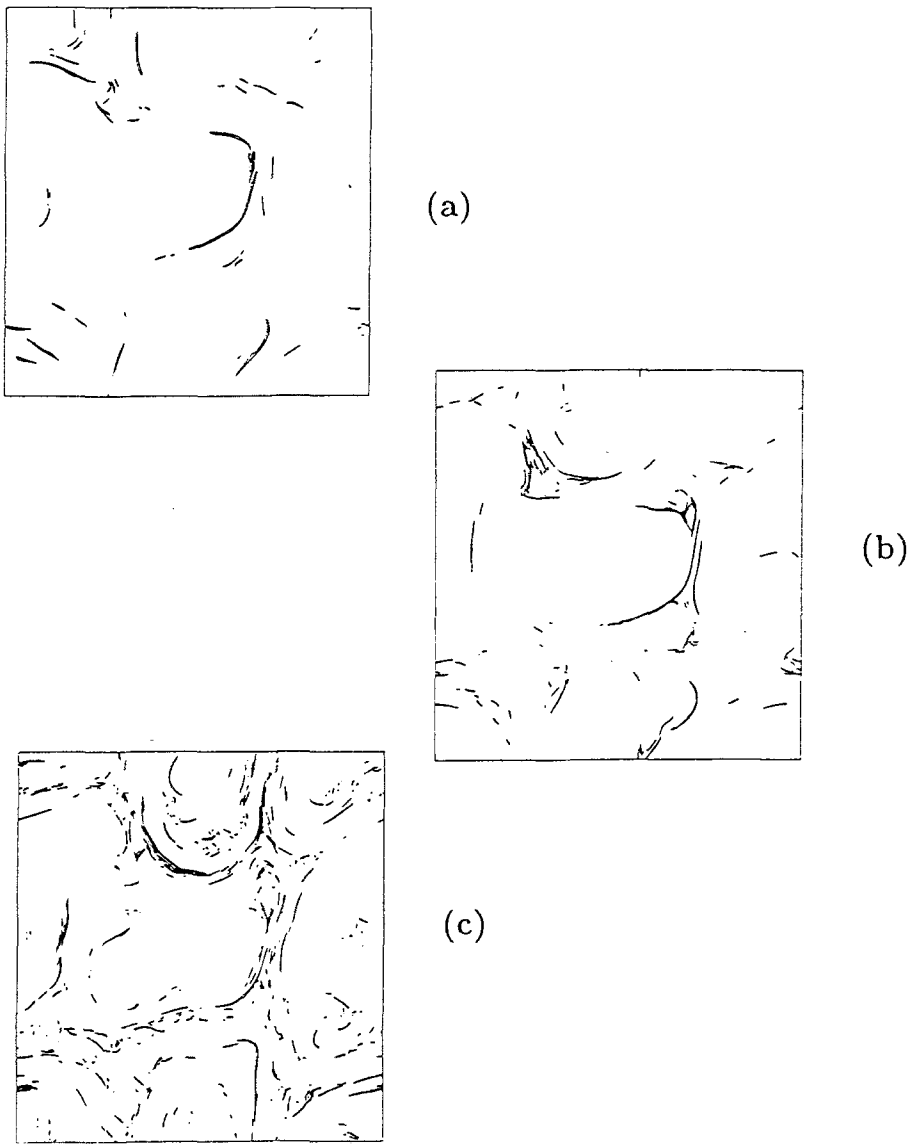

Figure 11. Distribution of micro-current sheets in 2D MHD turbulence for three different Reynolds numbers: (*a*) $R_m \simeq 12000$, (*b*) $R_m \simeq 25000$; (*c*) $R_m \simeq 50000$,for identical macro-states.

forteriori also expected to hold for 3D MHD turbulence. In fact recent numerical simulations of 3D MHD turbulence indicate, that dissipation is concentrated in sheet-like current and vorticity structures (Politano et al., 1995). Hence also with respect to the dissipation properties 2D and 3D systems seem to be rather similar.

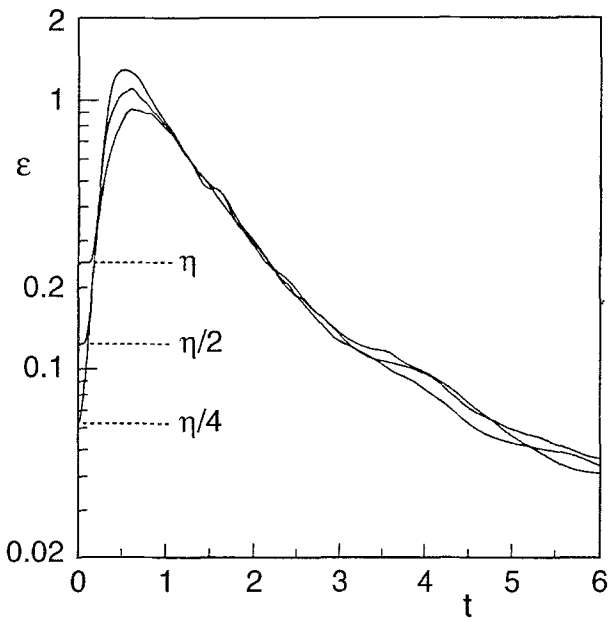

Figure 12. Energy dissipation rates $\varepsilon(t)$ in 2D decaying MHD turbulence of three simulation runs with different values of η.

The following picture of fast turbulent reconnection appears, illustrated in Fig. 13. MHD turbulence is preferentially excited in regions of strong current density (or current density gradients), i.e. around X-points, the natural loci of reconnection. Since in fully developed turbulence the energy dissipation rate is finite, independent of η, the magnetic field energy carried into the turbulent region is annihilated at a fast rate. This implies that the outside field is reconnected at the same rate.

5.3. The turbulent dynamo effect

While in the case of magnetized plasmas a 2D turbulence model may describe many features of the real 3D system, in primarily unmagnetized systems such as in stellar convection zones or accretion discs a fully 3D turbulence theory is required. In the case $W^M \ll W^V$ the analogy between the equation of motion (13) for $\boldsymbol{\omega}$, neglecting the Lorentz force, and the induction equation (14) for $\mathbf{B}$ indicates that $\mathbf{B}$ structures should be similar to $\boldsymbol{\omega}$ structures in Navier-Stokes turbulence, i.e. $\mathbf{B}$ should be concentrated in small-scale rope-like eddies. Concerning spectra one can argue that the magnetic energy spectrum

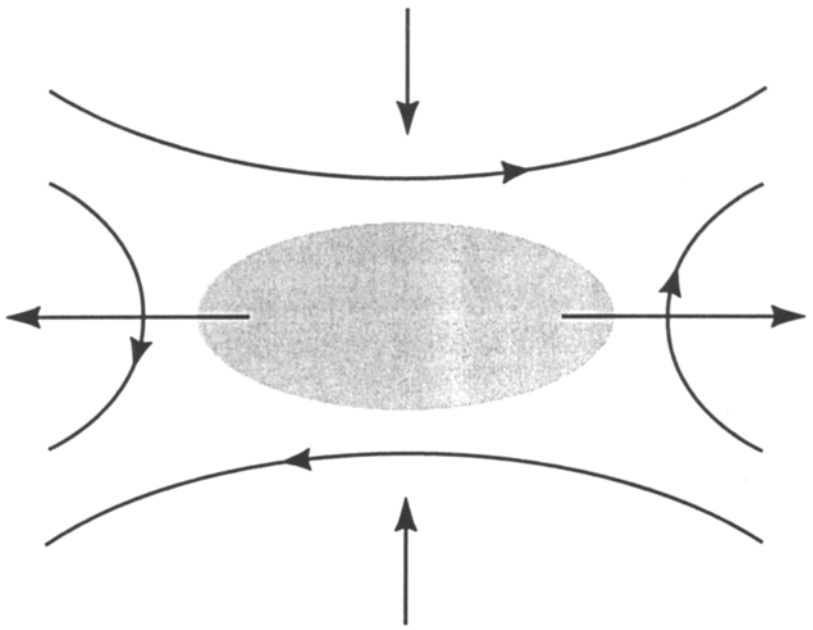

Figure 13. Schematic view of fast turbulent reconnection.

W_k^M should be similar to the vorticity spectrum $\Omega_k = k^2 W_k^V$

$$W_k^M \propto k^2 W_k^V \simeq \varepsilon^{2/3} k^{1/3}, \tag{67}$$

assuming a Kolmogorov law for the velocity spectrum W_k^V. Hence the magnetic spectrum for $W_k^M \ll W_k^V$ is fundamentally different from the $k^{-3/2}$ spectrum for MHD turbulence with $W^M \sim W^V$

The analogy between $\boldsymbol{\omega}$ and $\mathbf{B}$ can, however, only give the shape of the magnetic spectrum not its magnitude, in particular, cannot determine, whether a weak seed field will grow or decay. Starting from a smooth seed field distribution, W^M will always grow initially owing to field line stretching and twisting much as vortex line stretching in Navier-Stokes turbulence. Because of mass and magnetic flux conservation a flux tube stretched by a factor A shrinks in diameter as $d \propto A^{-1/2}$, while the field intensity increases as $B \propto A$, such that the magnetic energy enclosed in the tube increases as $W^M \propto A^2$. If the tube diameter becomes small enough, resistive dissipation may dominate over the convective stretching effect leading to subsequent decay of W^M. This always happens in 2D, where only a temporary dynamo effect is possible (Biskamp and Welter, 1990). In 3D such behavior is possible for $Pr_m \ll 1$. In the opposite case $Pr_m > 1$, where the viscous dissipation scale is larger than the resistive one, magnetic energy increase may continue, until the Lorentz force becomes important lead-

ing to dynamic saturation. This saturation occurs for $W_k^M \sim W_k^V$ at the smallest scales. In this state the total magnetic energy is still small compared with the fluid energy because of the spectrum (67). The final saturation level depends on Pr_m, see 3D simulations by Yanase et al. (1991).

The picture of magnetoconvection given so far describes the process of small-scale field excitation. Flux ropes are swirled around in a spaghetti-like manner, until the magnetic tension is large enough to slow down the swirling motion. Magnetic tension may also be reduced by flux rope reconnection. Reconnection plays an important role in the build-up of *large-scale* fields - the proper topic of dynamo theory - which can already be seen from the kinematic theory in mean-field electrodynamics (Steenbeck et al., 1966). Here $\mathbf{v}$ and $\mathbf{B}$ are split into large-scale mean parts and small-scale fluctuating parts, and the equation for $\widetilde{\mathbf{B}}$ is linearized

$$\partial_t \widetilde{\mathbf{B}} - \nabla \times (\mathbf{v}_0 \times \widetilde{\mathbf{B}}) = \nabla \times (\mathbf{v} \times \mathbf{B}_0) \,, \tag{68}$$

which obviously violates exact flux conservation. Averaging over small scales yields the well-known equation of turbulent dynamo theory

$$\partial \mathbf{B}_0 - \nabla \times (\mathbf{v}_0 \times \mathbf{B}_0) = -\nabla \times \mathbf{E} \,, \tag{69}$$

where

$$\mathbf{E} \;=\; -\langle \widetilde{\mathbf{v}} \times \widetilde{\mathbf{B}} \rangle \;\simeq\; \alpha \mathbf{B}_0 + \beta \nabla \times \mathbf{B}_0 \,, \tag{70}$$

$$\alpha = \tfrac{1}{3}\tau \langle \widetilde{\mathbf{v}} \cdot \nabla \times \widetilde{\mathbf{v}} \rangle, \;\; \beta = \tfrac{1}{3}\tau' \langle \widetilde{\mathbf{v}}^2 \rangle \,, \tag{71}$$

and $\tau \simeq \tau'$ are velocity correlation times. While β is positive representing a turbulent resistivity, which leads to a field energy decrease, α, which can have both signs depending on the kinetic helicity, may lead to field amplification. We thus find that dynamo action requires sufficiently complicated flows, which in particular should not be reflectionally symmetric, excluding dynamo action in 2D. Since the dynamics and statistics of the velocity field entering the coefficients α, β are assumed to be independent of $\mathbf{B}_0$, eq. (70) is only valid for sufficiently weak fields. For finite $\mathbf{B}_0$ small-scale fluctuations become Alfvén waves with $\widetilde{\mathbf{v}} \times \widetilde{\mathbf{B}} \simeq 0$. As a consequence the α-term is reduced. There is, however, a different process, leading to a nonlinear turbulent dynamo effect (Pouquet et al., 1976). Since small-scale fields $\widetilde{\mathbf{B}}$ are in general connected with small-scale magnetic helicity H_k^A, the inverse cascade of H_k^A leads to the build-up of large-scale magnetic fields. 3D simulations showing this effect have been performed by Meneguzzi et al. (1981).

In inhomogeneous systems strong large-scale fields may be generated by spatially separating the region of primarily kinetic turbulence from

the adjacent region, into which large-scale magnetic flux is transported and thus accumulated. Such a process seems to occur in the solar convection zone, where strong fields, which could be responsible for the solar dynamo effect, are concentrated in the stable overshoot region at the bottom of the convection zone (Nordlund et al., 1992).

6. Quasi-collisionless reconnection

In many hot, dilute plasmas, both in the laboratory and in space, Coulomb collisions are very weak, such that the nondissipative terms in **R**, eq. (9), are larger than the dissipative ones. This happens if typical resistive (or viscous) scales $\delta \sim \eta^{1/2}$ become smaller than the length scales characterizing the collisionless terms d_i, the ion inertia scale, or $d_i\beta = \rho_s$, the ion Larmor radius. From eq. (9) we see that for magnetized plasmas ($\beta < 1$) the $\mathbf{j} \times \mathbf{B}$ term, called the Hall term, is formally the most important collisionless effect. We should, however, note that the Hall term by itself cannot give rise to reconnection, since it simply restates the property of flux conservation in more precise form, the field being frozen to the electron flow instead of the mass flow. In fact it appears that also the remaining two nondissipative terms in **R** associated with electron pressure and electron inertia do not permit quasi-stationary reconnection. Hence some amount of dissipation is required, which, however, need not be due to Coulomb collisions but can also be caused by collisionless dissipation such as Landau damping. The important point is, that the reconnection dynamics, in particular the time scales, no longer depend on these weak dissipation processes.

In the low-β regime, to which I restrict myself, the pressure term in **R** is negligible. The inertia term, though formally very small, has a somewhat different quality and will hence be kept. The nondissipative terms change the dispersion properties of the plasma at small scales. Inserting **E** into Faraday's law and linearizing the latter together with the equation of motion (6) gives the dispersion relation

$$\omega^2 = k_{||}^2 v_A^2 \frac{1 + k^2 d_i^2}{(1 + d_e^2 k^2)^2} \,. \tag{72}$$

While at large scales $kd_i < 1$ we recover the dispersion-free Alfvén wave $\omega^2 = k_{||}^2 v_A^2$, waves become strongly dispersive at smaller scales, for $d_i^{-1} < k < d_e^{-1}$, called the whistler mode,

$$\omega^2 = (\Omega_e d_e^2)^2 k_{||}^2 k^2, \tag{73}$$

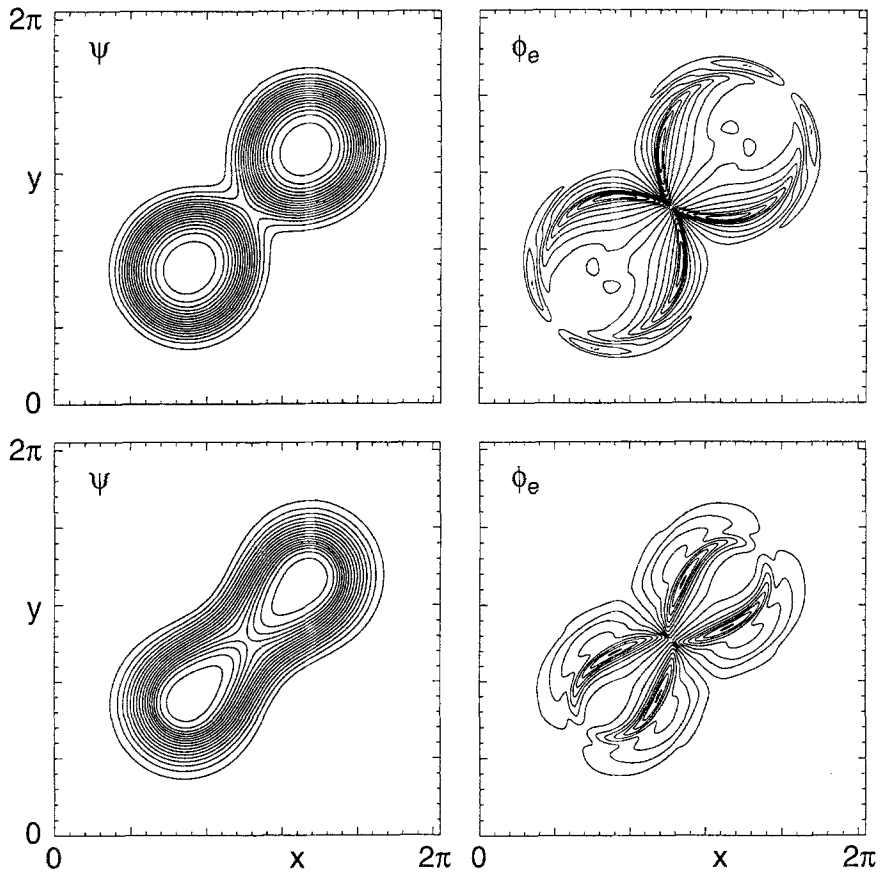

Figure 14. Coalescence of flux bundle in EMHD. Contours of ψ and ϕ_e, at two different times.

and for $kd_e > 1$, called the electron cyclotron mode,

$$\omega^2 = \Omega_e^2 k_{||}^2 / k^2. \tag{74}$$

While for the whistler mode the group velocity increases with k, $\partial\omega/\partial k \propto k$, reaching a maximum value $\sim \Omega_e d_e$, it drops to zero for the electron cyclotron mode, due to electron inertia. Note that the whistler is independent of both ion and electron inertia.

6.1. Electron magnetohydrodynamics

Let us first restrict consideration to scales smaller than d_i, where the ion dynamics can be neglected, the ions forming an immobile charge-neutralizing background. The dynamics is determined by the electron velocity $\mathbf{v}_e = -\mathbf{j}/ne$ and the selfconsistent magnetic field, following the equations

$$\partial_t(\mathbf{B} - d_e^2\nabla^2\mathbf{B}) - \nabla \times [\mathbf{v}_e \times (\mathbf{B} - d_e^2\nabla^2\mathbf{B})] = -\mu_e\nabla^{(4)}\mathbf{B}, \tag{75}$$

$$\mathbf{v}_e = -\alpha\nabla \times \mathbf{B}, \tag{76}$$

where $\alpha = c/4\pi ne$ is the Hall parameter. Equations (75), (76) are called electron magnetohydrodynamics (EMHD) (e.g. Kinsep et al., 1990). Linearization gives the whistler dispersion relation (72) (in the limit $kd_i > 1$). Since neglecting the ion dynamics corresponds to $m_i \to \infty$, i.e. $t_A \to \infty$, we have to use a different time unit, a convenient one being the whistler time $t_w = L^2/\Omega_e d_e^2 (= t_A/d_i)$, which formally corresponds to setting $\alpha = 1$ in eq. (76). On the right side of eq. (75) electron viscosity is chosen as the relevant dissipation process, since resistivity (= electron friction) can in general not prevent the formation of singular gradients.

Whistler modes are destabilized by a strong current density gradient (Mikhai-lovskii, 1974), where the most unstable modes are perpendicular to $\mathbf{j}$, i.e. to $\mathbf{B}$ in a low-β plasma. This suggests to study whistler-related processes in the poloidal plane perpendicular to $\mathbf{B}_0 = B_0\hat{\mathbf{z}}$. The 2D EMHD equations can be written (as in 2D incompressible MHD, note that $\nabla \cdot \mathbf{v}_e \propto \nabla \cdot \mathbf{j} = 0$) in terms of a flux function ψ, $\mathbf{B}_p = \hat{\mathbf{z}} \times \nabla\psi$ and a stream-function ϕ_e, which is the axial field fluctuation, $\mathbf{v}_e = \hat{\mathbf{z}} \times \nabla\phi_e = \hat{\mathbf{z}} \times \nabla B_z$:

$$\partial_t(\psi - d_e^2 j) + \mathbf{v}_e \cdot \nabla(\psi - d_e^2 j) = -\mu_e\nabla^2 j, \tag{77}$$

$$\partial_t(\phi_e - d_e^2\omega_e) + \mathbf{v}_e \cdot \nabla(\phi_e - d_e^2\omega_e) + \mathbf{B}_p \cdot \nabla j = -\mu_e\nabla^2\omega_e, \tag{78}$$

$$j = \nabla^2\psi, \ \omega_e = \nabla^2\phi_e. \tag{79}$$

Let us consider stationary reconnection in the framework of eqs. (77), (78). For $d_e = 0$ and $\mu_e = 0$ and stationary conditions the equations reduce to

$$\mathbf{v}_e \cdot \nabla\psi = -E, \tag{80}$$

$$\mathbf{B}_p \cdot \nabla j = 0 \tag{81}$$

with $\partial_t\psi = E = \text{const.}$, which have the similarity solution

$$\psi = \tfrac{1}{2}(x^2 - a^2y^2), \tag{82}$$

$$\phi_e = \tfrac{1}{2}\frac{E}{a}\ln\left|\frac{x+ay}{x-ay}\right| . \tag{83}$$

The solution corresponds to an upstream flow converging toward the X-point and downstream flow diverging away from it. Finite dissipation is needed to smooth the flow singularity along the separatrix $x = \pm ay$. In the vicinity of the neutral point electron inertia must be retained and ψ and ϕ_e deviate from the solution (82), (83). A micro-current layer of length $\Delta \sim (Ed_e^2)^{1/3}$ and width $\delta \sim d_e$ is driven by the applied field E. One can show, that the integrated current in this layer goes to zero for $d_e \to 0$. Thus the magnetic field at the X-point retains its structure (82) for any E, the latter depending only on the external configuration, i.e. on the free magnetic energy of the system, in contrast to the resistive MHD case, where reduction of the smallness parameter η leads to a macroscopic current sheet and small $E = O(\eta^{1/2})$. To illustrate these results let me present some numerical simulations of the 2D EMHD equations. I consider the coalescence of two magnetic flux bundles as shown in Fig. 14. The conspicuous feature is, that flux surfaces appear to be pulled into the X-point instead of pushed against it as in the MHD case (see the MHD coalescence system, Fig. 8). This behavior is caused by the structure of the flow with streamlines converging (i.e. velocity increasing) toward the X-point, which is consistent with the solution (83). The reconnection rate is found to be independent of d_e and also of the dissipation coefficient μ_e, as long as the latter is not too large. For very small μ_e quasi-singular substructures inside the current layer are generated corresponding to cusp-like electron flow (or current) profiles. The collimated outflow finally becomes Kelvin-Helmholtz unstable generating turbulence, which is convected out from the reconnection region into the downstream cone. The turbulence gives a natural mechanismfor a finite energy dissipation rate in the limit $\mu_e \to 0$. Turbulence generation is found to be much more efficient than the generation of Alfvén turbulence in the case of resistive current sheets.

While the 2D EMHD model (77), (78) gives a good approximation for laminar quasi-stationary processes, they cannot adequately describe the dynamics, when turbulence gets in. In 3D turbulence is more violent because of modes with finite k_z excited by the z-component of the current density at the X-point. 3D simulations of unstable current layers in the framework of EMHD have recently been performed (Drake et al., 1994) indicating excitation of rather isotropic turbulence, which broadens the current layer to a width exceeding d_e. The effect of the turbulence can be described by a turbulent electron viscosity $\mu_{eff} = a\Omega_e d_e^2$, where the numerical coefficient is $a \sim 0.1$.

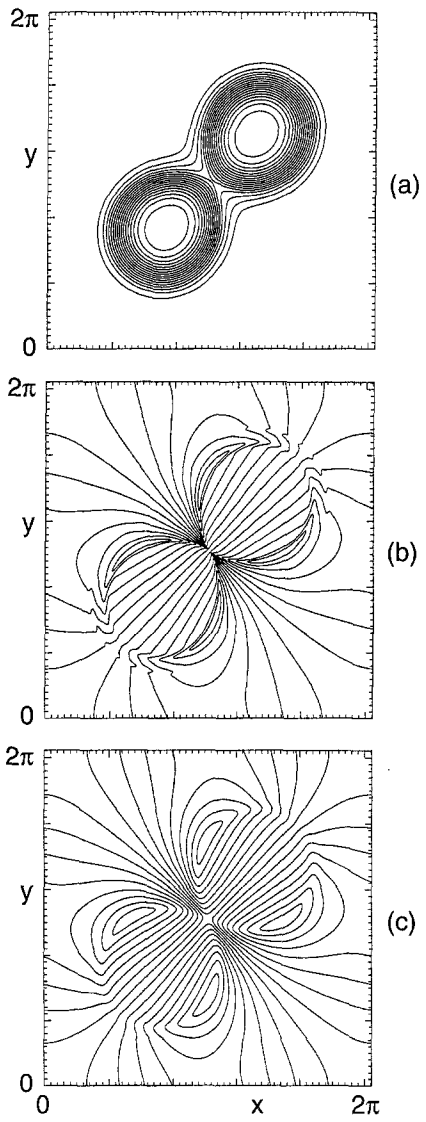

Figure 15. Coalescence of flux bundles as in Fig. 14, but including the ion motion.

6.2. Ion controlled quasi-collisionless reconnection

At spatial scales exceeding d_i the ion motion can no longer be neglected. Here ions and electrons move essentially together, which justifies neglecting the Hall term in the MHD approximation. I include the ions in a simple model assuming their motion to be incompressible. In the 2D case the ion velocity is hence given in terms of a stream-function

$\phi_i, \mathbf{v}_i = \hat{\mathbf{z}} \times \nabla\phi_i$, $\omega_i = \nabla^2\phi_i$. Adding the equations of motion for ions and electrons we obtain

$$d_i^2(\partial_t\omega_i + \mathbf{v}_i \cdot \nabla\omega_i) + d_e^2(\partial_t\omega + \mathbf{v}_e \cdot \nabla\omega_e) - \mathbf{B} \cdot \nabla j = \mu_i\nabla^2\omega_i + \mu_e\nabla^2\omega_e. \quad (84)$$

Neglecting the axial velocity of the ions compared with that of the electrons, the axial current density $j_z = j$ remains unchanged and hence eq. (77) for ψ. The poloidal current density is, however, modified by the ion motion, $\mathbf{j}_p = -\hat{\mathbf{z}} \times \nabla B_z = \hat{\mathbf{z}} \times \nabla(\phi_i - \phi_e)$. Hence eq. (78) becomes

$$\partial_t(\phi_e - \phi_i - d_e^2\omega_e) + \mathbf{v}_e \cdot \nabla(\phi_e - \phi_i - d_e^2\omega_e) + \mathbf{B} \cdot \nabla j = -\mu_e\nabla^2\omega_e. \quad (85)$$

In this equation the term $B_z\nabla \cdot \mathbf{v}_e$ has been neglected by assuming exact incompressibility $\nabla \cdot \mathbf{v}_i = 0$. While this is rigorous in EMHD since $\mathbf{v}_e = -\mathbf{j}$ and $\nabla \cdot \mathbf{j} = 0$, including the ion motion this approximation requires that $B_z\nabla \cdot \mathbf{v}_i$ is small, i.e. that $\nabla \cdot \mathbf{v}_i$ is small independent of the presence of a strong axial field, which can be proved only for a large background pressure, i.e. for high-β, since finite $dp_i/dt = -\gamma p_i \nabla \cdot \mathbf{v}_i$ enforces $\nabla \cdot \mathbf{v}_i \simeq 0$ if p_i is large. The low-β behavior is presently under investigation.

Numerical simulations of flux tube coalescence for $d_i < 1$ using eqs. (77), (84), (85) (Biskamp et al., 1995) show that the reconnection rate E is independent of the electron parameters d_e, μ_e, as could be expected from the EMHD results presented in section 6.1. E depends only on d_i, i.e. on the ion mass. Figure 15 gives a typical state during the coalescence process with $d_i = 0.1, d_e = 0.015$. It can be seen by comparing ϕ_e and ϕ_i contours, that at finite distances from the X-point (and the separatrix) ion and electron flow patterns are very similar. They differ, however, in the vicinity of the X-point, where ion spatial scales ($\sim d_i$) are much larger than those of the electrons ($\sim d_e$). For $|\mathbf{x}| < d_i$ the electron flow again shows the converging pattern as in the EMHD case.

For not too small values of d_i, $d_i \gtrsim 0.1$, one finds that E has an Alfvénic scaling. For smaller values of $d_i, d_i < 0.1$ the reconnection configuration assumes the shape of an elongated sheet of width d_i corresponding to $E \sim d_i v_A$, which for $d_i \ll 1$ is slower than Alfvénic, but still much larger than $E \sim d_e v_A$, as would be obtained neglecting the Hall term, which would imply forcing also the ions into a narrow channel of width d_e. In addition the elongated current layer is prone to plasmoid generation as in the resistive case, which further increases the reconnection rate.

7. Conclusions

I have presented an overview of the present status of the theory of magnetic reconnection in plasmas. In the conventional framework of resistive MHD reconnection at intermediate magnetic Reynolds numbers R_m takes place in quasi-stationary current sheets, so-called Sweet-Parker sheets, of macroscopic length giving rise to reconnection rates $E = O(\eta^{1/2})$, which are far too slow if extrapolated to the large R_m values in many astrophysical systems. This extrapolation is, however, not legitimate, since at high R_m reconnection occurs in a turbulent way. Fully developed MHD turbulence seems to allow finite reconnection rates in the limit $\eta \to 0$. The effect of the turbulence can be modelled by assuming a localized anomalous resistivity, as done in many simulations of substorms or flares.

Primarily nondissipative reconnection processes dominate in hot, dilute plasmas, where collisional effects are negligibly small. In fact parameters such as the Reynolds number lose their relevance to characterize the dynamics in quasi-collisionless systems because of the presence of much more effective collisionless processes. Hence one has to broaden the theoretical framework by including nondissipative terms in Ohm's law, above all the Hall term and electron inertia. It is found that reconnection rates are independent of electron inertia and also of the value of the residual dissipation coefficients, depending only on the ion mass. Small-scale whistler turbulence is easily excited in the reconnection region giving rise to anomalous electron viscosity.

I have not touched on kinetic effects, in particular collisionless dissipation due to resonant wave-particle interactions such as Landau or cyclotron damping. Inverse Landau damping can give rise to microinstabilities. A well-known example is the ion-sound instability driven by a sufficiently high current density in a plasma with temperature ratio $T_e/T_i > 1$, which generates small-scale electrostatic turbulence. Little is known about the efficiency of particle acceleration to high energies by reconnection processes. Ion acceleration is mainly bulk plasma acceleration up to the Alfvén speed. Electrons may be accelerated by the inductive field E in the reconnection region, but simple estimates predict that the period electrons stay in the region where they can be freely accelerated, are short (Biskamp and Schindler, 1971), in particular if the reconnection region is turbulent. The acceleration has probably a rather low efficiency depending strongly on the local coherence properties of the magnetic configuration, much in contrast to the robustness of the diffusive shock acceleration.

I have also not talked about sudden onset conditions of reconnection processes. This is a general problem which always arises, when trying

to explain an eruptive process by a linear instability. It appears that in many cases the fast excitation of small-scale turbulence is a probable mechanism acting as a quasi-instantaneous switch-on of a high resistivity. With the advent of extremely powerful parallel computers high resolution numerical simulations in fully 3D geometry will shed more light on these still unexplored areas.

References

Amo, H., T. Sato, and A. Kageyama, 1994, Intermittent energy bursts and recurrent topological change of a twisted magnetic flux tube, National Institute for Fusion Science, Res. Report NIFS-309, Nagoya, Japan

Braginskii, S. I., 1965, Transport processes in a plasma, Reviews of Plasma Physics, ed. M. A. Leontovich (Consultants Bureau, New York), Vol. 1, 205-311

Birn, J., and E. W. Hones, Jr., 1981, Three-dimensional computer modeling of dynamic reconnection in the geomagnetic tail, J. Geophys. Res. **86**, 6802 - 6808

Biskamp, D., 1986, Magnetic reconnection via current sheets, Phys. Fluids **29**, 1520-1531

Biskamp, D., 1991, Algebraic nonlinear growth of the resistive kink instability, Phys. Fluids **B3**, 3353-3356

Biskamp, D., 1993, Nonlinear Magnetohydrodynamics (Cambridge University Press, Cambridge)

Biskamp, D., and U. Bremer, 1993, Dynamics and statistics of inverse cascade processes in 2D magnetohydrodynamic turbulence, Phys. Rev. Lett. **72**, 3819 - 3822

Biskamp, D., and K. Schindler, 1971, Instability of two-dimensional collisionless plasmas with neutral points, Plasma Phys. **13**, 1013-1026

Biskamp, D., and H. Welter, 1980, Coalescence of magnetic islands, Phys. Rev. Lett. **44**, 1069-1072

Biskamp, D., and H. Welter, 1989a, Dynamics of decaying two-dimensional magnetohydrodynamic turbulence, Phys. Fluids B **1**, 1964-1979

Biskamp, D., and H. Welter, 1989b, Magnetic arcade evolution and instability, Solar Phys. **120**, 49-77

Biskamp, D., and H. Welter, 1990, Magnetic field amplification and saturation in two-dimensional magnetohydrodynamic turbulence, Phys. Fluids **B 2**, 1781-1793

Biskamp, D., E. Schwarz, and J. F. Drake, 1995, Ion-controlled collisionless magnetic reconnection, submitted to Phys. Rev. Lett.

Bulanov, S. V., J. Sakai, and S. I. Syrovatskii, 1979, Tearing mode instability in approximately steady MHD configurations, Sov. J. Plasma Phys. **5**, 157-163

Burlage, L. F., and J. M. Turner, 1976, Microscale Alfvén waves in the solar wind at 1 AU, J. Geophys. Res. **81**, 73-77

Cowley, S. W. H., 1975, Magnetic field line reconnection in a highly-conducting incompressible fluid: properties of the diffusion region, J. Plasma Phys. **14**, 475-490

Dobrowolny, M., A. Mangeney, and P. Veltri, 1980, Fully developed anisotropic hydromagnetic turbulence in interplanetary space, Phys. Rev. Lett. **45**, 144-147

Drake, J. F., R. G. Kleva, and M. E. Mandt, 1994, Structure of thin current layers: Implications for magnetic reconnection, Phys. Rev. Lett. **73**, 1251-1254

Elsässer, W. M., 1950, The hydromagnetic equations, Phys. Rev. **79**, 183

Fadeev, V. M., I. F. Kvartskhava, and N. N. Komarov, 1965, Self-focusing of local plasma currents, Nucl. Fusion **5**, 202-209

Furth, H. P., J. Killeen, and M. N. Rosenbluth, 1963, Finite resistivity instabilities of a sheet pinch, Phys. Fluids **6**, 459-484

Grappin, R., A. Pouquet, and J. Léorat, 1983, Dependence of MHD turbulence spectra on the velocity-magnetic field correlation, Astron. Astrophys. **126**, 51-58

Hautz, R., and M. Scholer, 1987, Numerical simulations on the structure of plasmoids in the deep tail, Geophys. Res. Lett. **14**, 969-972

Iroshnikov, P. S., 1964, Turbulence of a conducting fluid in a strong magnetic field, Sov. Astron. **7**, 566-571

Kageyama, A., K. Watanabe, and T. Sato, 1990, Global simulation of the magnetosphere with a long tail: The formation and ejection of plasmoids, National Institute of Fusion Studies, Res. Report NIFS-49, Nagoya, Japan

Kingsep, A. S., K. V. Chukbar, and V. V. Yan'kov, 1990, Electron magnetohydrodynamics, Reviews of Plasma Physics, ed. B. B. Kadomtsev (Consultants Bureau, New York), Vol. **16**, 243-288

Kraichnan, R. H., 1965, Inertial range spectrum in hydromagnetic turbulence, Phys. Fluids **8**, 1385-1387

Matthaeus, W. H., M. L. Goldstein, and C. Smith, 1982, Evaluation of magnetic helicity in homogeneous turbulence, Phys. Rev. Lett. **48**, 1256-1259

Matthaeus, W. H., and D. Montgomery, 1980, Selective decay hypothesis at high mechanical and magnetic Reynolds numbers, Ann. NY Acad. Sci. **357**, 203

Matthaeus, W. H., and D. Montgomery, 1984, Dynamic alignment and selective decay in MHD, in: Statistical Physics and Chaos in Fusion Plasmas, eds. W. Horton and L. Reichl (Wiley, New York), pp. 285-291

Meneguzzi, M., U. Frisch, and A. Pouquet, 1981, Helical and nonhelical turbulent dynamos, Phys. Rev. Lett. **47**, 1060-1064

Mikic, Z., D. C. Barnes, and D. D. Schnack, 1988, Dynamical evolution of a solar coronal magnetic arcade, Astrophys. J. **328**, 830-847

Mikhailovskii, A. B., 1974, Theory of Plasma Instabilities (Consultants Bureau, New York), Vol. 2, p. 63

Nordlund, A. A. Brandenburg, R. L. Jennings, M. Rieutord, J. Ruokolainen, R. F. Stein, and I. Tuominen, 1992, Dynamo action in stratified convection with overshoot, Astrophys. J. **392**, 647-652

Otto, A., K. Schindler, and J. Birn, 1990, Quantitative study of the nonlinear formation and acceleration of plasmoids in the earth's magnetotail, J. Geophys. Res. **95**, 15023-15037

Parker, E. N., 1963, The solar flare phenomenon and the theory of reconnection and annihilation of magnetic fields, Astrophys. J. Suppl. Ser. **8**, 177-211

Petschek, H. E., 1964, Magnetic field annihilation, AAS/NASA Symp. on the Physics of Solar Flares, ed. W. N. Hess (NASA, Washington, DC) pp. 425-437

Politano, H., A. Pouquet, and P. L. Sulem, 1995, Current and vorticity dynamics in three-dimensional MHD turbulence, Phys. Plasmas **2**, 2931-2939

Pouquet, A., U. Frisch, and J. Léorat, 1976, Strong MHD helical turbulence and the nonlinear dynamo effect, J. Fluid Mech. **77**, 321-354

Pritchett, P. L., and C. C. Wu, 1979, Coalescence of magnetic islands, Phys. Fluids **22**, 2140-2146

Rutherford, P. H., 1973, Nonlinear growth of the tearing mode, Phys. Fluids **16**, 1903-1908

Sato, T., and T. Hayashi, 1979, Externally driven magnetic reconnection and a powerful magnetic energy converter, Phys. Fluids **22**, 1189-1202

Steenbeck, M., F. Krause, and K. H. Rädler, 1966, Berechnung der mittleren Lorentz-Feldstärke $\langle \mathbf{v} \times \mathbf{B} \rangle$ für ein elektrisch leitendes Medium in turbulenter, durch Coriolis Kräfte beeinflusster Bewegung. Z. Naturforsch. **21a**, 369-376

Sweet, P. A., 1958, The production of high energy particles in solar flares, Nuovo Cimento Suppl. **8**, Ser. X, 188-196

Syrovatskii, S. I., 1971, Formation of current sheets in a plasma with a frozen-in strong magnetic field, Sov. Phys. - JETP **33**, 933-940

Syrovatskii, S. I., 1981, Pinch sheets and reconnection in astrophysics, Annu. Rev. Astron. Astrophys. **19**, 163-229

Taylor, J. B., 1986, Relaxation and magnetic reconnection in plasmas, Rev. Mod. Phys. **53**, 741-763

Waelbroeck, F. L., 1989, Current sheets and nonlinear growth of the $m = 1$ kink-tearing mode, Phys. Fluids **B 1**, 2372-2380

Woltjer, L., 1958, A theorem of force-free magnetic fields, Proc. Natl. Acad. Sci. (Washington) **44**, 489-492

Yanase, S., J. Mizushima, and S. Kida, 1991, Coherent structures in MHD turbulence and turbulent dynamo, in Turbulence and Coherent Structures, ed. O. Métais and M. Lesieur (Kluiver, Dordrecht), pp. 569-583